

5-18-1988

DC-excited cw CO₂ Metal Waveguide Laser

Fahad Saleh Al-Mashaabi
Portland State University

Follow this and additional works at: https://pdxscholar.library.pdx.edu/open_access_etds



Part of the [Electrical and Computer Engineering Commons](#)

Let us know how access to this document benefits you.

Recommended Citation

Al-Mashaabi, Fahad Saleh, "DC-excited cw CO₂ Metal Waveguide Laser" (1988). *Dissertations and Theses*. Paper 3756.

<https://doi.org/10.15760/etd.5641>

This Thesis is brought to you for free and open access. It has been accepted for inclusion in Dissertations and Theses by an authorized administrator of PDXScholar. Please contact us if we can make this document more accessible: pdxscholar@pdx.edu.

AN ABSTRACT OF THE THESIS OF Fahad Saleh Al-Mashaabi for the Master of Science in Electrical Engineering presented May 18, 1988.

Title: DC Excited cw CO₂ Metal Waveguide Laser

APPROVED BY THE MEMBERS OF THE THESIS COMMITTEE:



Lee W. Casperson, Chair



Faris Badi'i



Richard Morris



Carl Bachhuber

A novel design for a DC excited cw CO₂ metal waveguide laser has been developed in which a slotted hollow-cathode in a transverse discharge also doubles as a metal waveguide. This design has been implemented in a compact design that produces up to 1 watt of cw, 10.6 μm radiation. The discharge characteristics, laser gain and laser output has been studied as functions of various discharge parameters. The advantages of the new transverse discharge of the slotted hollow

cathode geometry include low voltage, positive impedance and high optical gain. Overall efficiency is comparable with those of conventional longitudinal CO₂ lasers. The output laser modes were very clean low order Gaussian modes.

**DC-EXCITED CW CO₂ METAL WAVEGUIDE
LASER**

by

FAHAD SALEH AL-MASHAABI

A thesis submitted in partial fulfillment of the
requirements for the degree of

**MASTER OF SCIENCE
in
ELECTRICAL ENGINEERING**

Portland State University

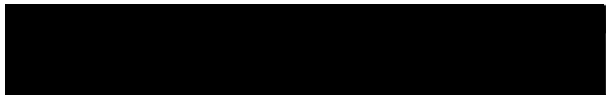
1988

TO THE OFFICE OF GRADUATE STUDIES:

The members of the Committee approve the thesis of Fahad Saleh Al-Mashaabi presented May 18, 1988.



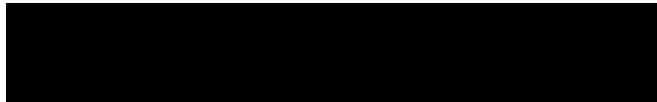
Lee W. Casperson, Chair



Faris Badi'i

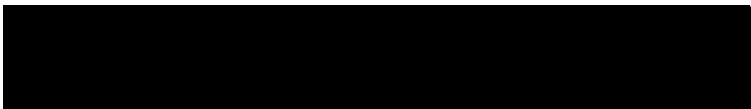


Richard Morris



Carl Bachhuber

APPROVED:



Lee W. Casperson, Chair, Department of Electrical Engineering



Bernard Ross, Vice Provost for Graduate Studies

ACKNOWLEDGEMENT

I am very grateful for the guidance and support of Professor Lee Casperson throughout the duration of this research. I also wish to thank Duncan McFarlane and Manuela Fe Tarroja for their meaningful suggestions; Shirley Clark for her patience in proof reading my thesis; and the other members of the laser research group for helping to provide an exciting atmosphere for research.

I wish also to thank my parents and Michele Provost and all my friends for their help, moral support, and encouragement.

TABLE OF CONTENTS

	PAGE
ACKNOWLEDGEMENT	iii
TABLE OF CONTENT	iv
LIST OF FIGURES	vi
CHAPTER I: INTRODUCTION	1
Introduction	1
Description of the Device	3
Applications	5
CHAPTER II: CO ₂ LASER	6
Introduction	6
Molecular Spectra	6
Excitation Processes	12
CHAPTER III: LASER DISCHARGE	20
Introduction	20
Glow Discharge	21
Hollow-Cathode Glow Discharge	28
Slotted Hollow-Cathode Discharge	33

CHAPTER IV: GAIN MEASUREMENT	37
Introduction	37
Theory	38
Gain Measurement Apparatus	40
Results of Gain Measurements	43
CHAPTER V: METAL WAVEGUIDE LASER	54
Introduction	54
Waveguide Transverse Modes	54
Output Power	60
CHAPTER VI: CONCLUSION AND RECOMMENDATIONS	63
Conclusion	63
Recommendations for Future Work	64
REFERENCES	65

LIST OF FIGURES

FIGURE	PAGE
1-1. DC Exited CO ₂ Metal Waveguide Laser.	4
2-1. Energy level diagram of the CO ₂ : N ₂ : He laser	7
2-2. Energy level diagram of the CO ₂ molecule	11
2-3. Energy dependence of elastic and inelastic cross sections in CO ₂	13
2-4. Momentum transfer and inelastic cross sections for electrons in CO ₂ derived from electron transport coefficients	13
2-5. Cross section for the first vibrational level (v = 1) excitation of N ₂ by electron impact	14
2-6. Total effective Cross section for vibrational excitation of N ₂ (v = 1-8) by electron impact (ref.[13]).	14
2-7. Fraction of power transferred from the electrons	15
3-1. Voltage-current relation of low pressure gaseous gap	22
3-2. The normal glow discharge in neon in a 50 cm tube at 1 torr	24
3-3a. Parallel-plane cathode discharge system configuration	29
3-3b. Slotted hollow cathode discharge system configuration	29
3-4. Voltage-current characteristics of the waveguide discharge	36
4-1. Gain measurement apparatus	42

4-2.	Gain as a function of He/CO ₂ ratio at 7 Torr	45
4-3.	Gain as a function of N ₂ /CO ₂ ratio at 7 torr	46
4-4.	Gain as a function of pressure	47
4-5.	Gain profile for the gas mixture 1:3.2:14.2 at 7 torr	48
4-6.	Gain profile for the gas mixture 1:3.2:14.2 at 6.5 torr	49
4-7.	Gain profile for the gas mixture 1:3.2:18 at 7 torr	50
4-8.	Gain profile for the gas mixture 1:3.2:8 at 7 torr	51
4-9.	Gain profile for the gas mixture 1:3.2:8 at 6 torr	52
5-1.	Waveguide coordinate system.	57
5-2.	Normalized intensity profile for the second order Hermite-Gaussian mode	58
5-3.	Normalized intensity profile for the second order Airy mode	58
5-4.	First order Hermite-Gaussian output mode	59
5-5.	Laser power as a function of current for different gas mixtures at 7 torr	61
5-6.	Laser power as a function of current for the gas mixture 1:3.2:14.2 at 7 torr and 10 torr.	62

CHAPTER I

INTRODUCTION

Demand for the development of infrared optical waveguides to deliver CO₂ laser beams to a target, has led researchers to investigate two types of waveguides, the flexible metal [1,2,3] and the infrared fiber-optical [4,5] waveguides. There are often clear advantages to using a fiber optic waveguide for low power application, but for high-power applications metallic waveguides have proved to be the best choice.

A metallic waveguide could be a hollow tube [1] or a concave strip [2]. In order to efficiently couple laser beams into either type of waveguide, Marhic [3] proposed a laser whose output modes match the waveguide modes. This is done in such a way that the walls of the laser active medium are made up of a portion of the waveguide itself or has a similar shape to it. Resonators of this type have been experimentally studied, and examples are the cw CO₂ laser with a slightly bent glass tube [3] and the transversely RF-excited metal waveguide laser [6] with a concave metal strip waveguide. Although the output modes of both lasers have been shown to agree well with the expected Airy-Hermite-Gaussian functions, there are practical differences between the two schemes. The glass tube laser suffers from very inefficient use of the gain medium. The second laser is more efficient but is more expensive because it requires a RF power supply, which complicates matters because it requires impedance matching between the RF power supply and the laser discharge which is hard to obtain. These problems may be

simultaneously eliminated by carefully designing a new type of waveguide discharge that is able to generate a relatively high gain medium using DC excitation.

The focus of this thesis is to develop a novel design of high gain transversely DC excited metal waveguide laser. This new type of waveguide laser has been constructed and investigated. The design of this waveguide laser device is described in the next section of this chapter.

In chapter II, a brief discussion of the molecular spectra and the excitation processes is presented. Understanding these processes is a prerequisite for finding the right discharge conditions for laser gain which demands knowing the role of each gas and their interactions in an electrical discharge. Chapter III will introduce the low pressure glow discharge and finally focuses on the discharge characteristics of our slotted hollow-cathode waveguide.

In chapter IV, the gain measurement, which is a necessary step in assessing the suitability of our new waveguide discharge for laser excitation and in obtaining the optimum discharge conditions for laser action, is presented. Next, the above amplifier is turned into a laser medium by placing it inside an optical resonator. In chapter V, The operation of this laser is studied by observing the transverse output modes and measuring the output power as functions of different discharge conditions.

DESCRIPTION OF THE DEVICE

A new slotted hollow metal tube which serves both as a cathode and a waveguide in a transverse discharge has been developed in this work. The new waveguide discharge is unique and has almost the same characteristics of both plane-cathode and hollow-cathode discharges. The discharge voltage is low being on the order of 370-450 volts. Also, the discharge exhibits a positive impedance. As a result, the over-all efficiency is increased, since very small or zero ballast resistance can be used. The optical gain measurements revealed a substantial gain available and lasing has been achieved.

This novel DC transversely-excited metal waveguide laser consists (as shown in fig. 1-1) of three main parts, the cathode (waveguide), the anode and the resonator structure.

The cathode material and shape is a simple copper tube (ID = 1.1 cm) which is being slotted along its center axis with a slot width of .9 cm. The cathode is also bent manually along the optical axis to have the desired radii of curvature. Copper is chosen for its excellent $10.6 \mu\text{m}$ optical properties, low work function and low susceptibility to sputtering [24]. The polished inner surface of the cathode has also retained its surface cleanliness during the whole operation, thus, lowering even more the susceptibility to sputtering and eliminating the need for the toxic and expensive BeO (Beryllium Oxide) or other materials such as Al_2O_3 (Aluminium Oxide) and BN (Boron nitride) which are used as waveguide walls. Cooling of the copper cathode in our design is provided by tap water that flows through a small diameter copper pipe (ID = .5 cm) attached to the outer surface of the cathode.

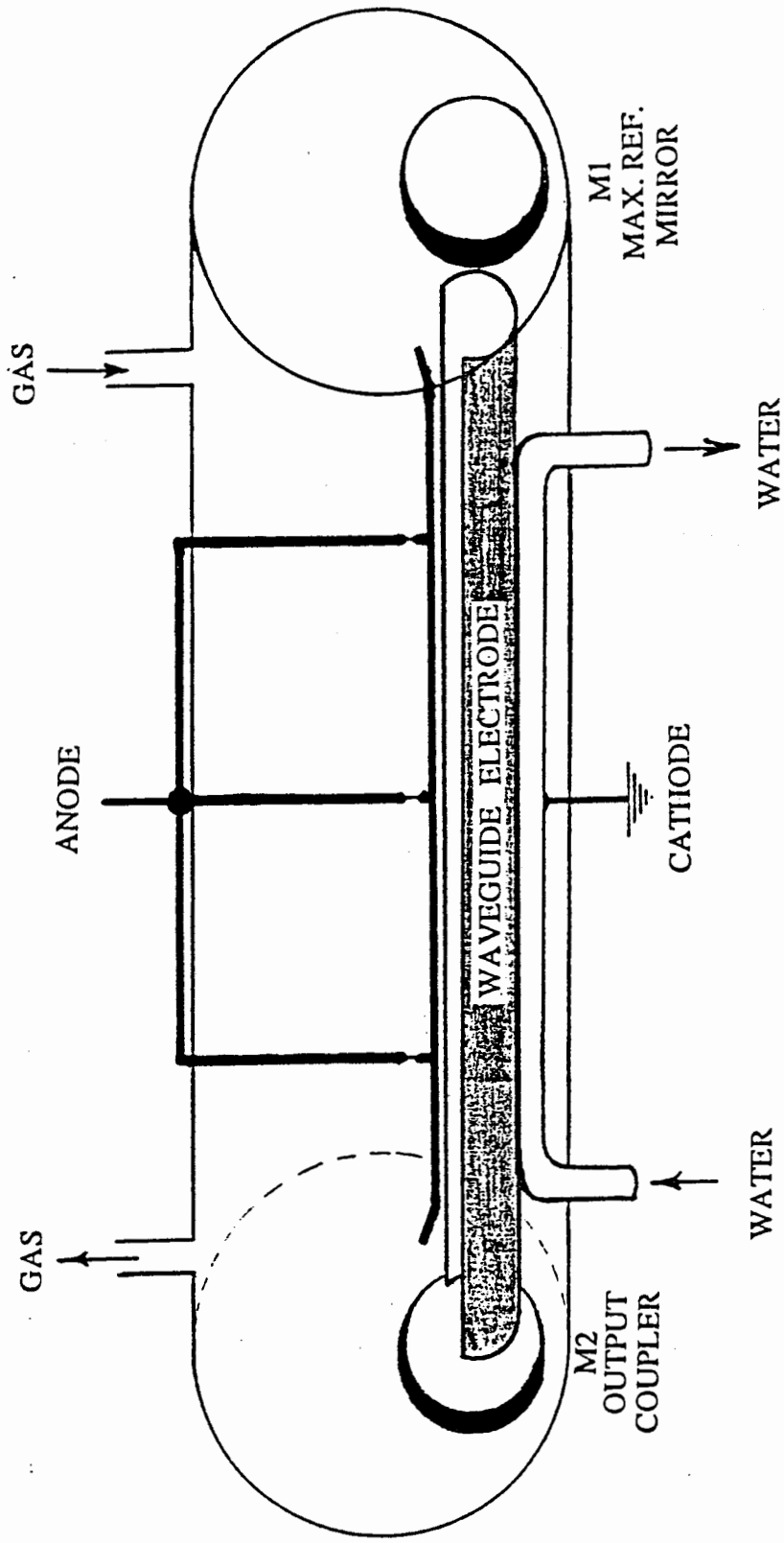


Figure 1-1. DC Exited CO₂ Metal Waveguide Laser

The anode material of this device is not critical and no noticeable differences in the V-I characteristics were observed when different metals were tested. The anode principally used during the experiment was a 3 mm diameter brass rod. The anode is supported by another three rods through hinged connections that allow the matching of the anode's radius to the major radius of curvature of the cathode.

The resonator structure was inclosed in a vacuum tight plexi-glass tube (ID = 3.5 in, OD = 4 in) that is O-ring sealed at both ends with plexi-glass plates. These two boards hold the two adjustable mirrors mounts.

This device was connected to a power supply of (1.0 kV, 1.5 A) to sustain the discharge. Although the discharge has a positive impedance, a low 1 k Ω ballast resistor is used to stabilize the discharge and to protect the power supply from sudden arcs caused by any defects on the cathode surface. The ratio of the input gas mixture of CO₂ : N₂ : He was controlled by three (1 standard cubic foot per hour [SCFH]) Dwyer flow meters. The flow rate of the gas mixture was kept constant at approximately 1 SCFH.

APPLICATIONS

The compact size, rugged structure, positive impedance and good model quality makes this metal waveguide laser suitable for many applications, such as laser surgery, laser machining and laser radar. Further, this design could be used in all applications where dielectric waveguide CO₂ lasers or conventional longitudinal CO₂ lasers are currently in use.

CHAPTER II

CO₂ LASER

INTRODUCTION

The CO₂ laser is one of the most efficient and most studied of all lasers demonstrated to date. Cw CO₂ lasers with output of 50 kw have been reported, and pulses as short as 1 nsec have been measured. The CO₂ laser efficiency can be as high as 30 percent. The laser medium of CO₂ laser usually consists of either flowing CO₂ : N₂ : He or sealed-off CO₂ : N₂ : He : CO : Xe gas mixture. These mixtures can be excited by either a DC or an RF electrical discharge or in some cases by e-beam bombardment. Because of the number of different gases involved in the discharge, the CO₂ laser discharge is very complicated, however, many types of CO₂ laser discharges are now fairly well understood. In order to understand our particular waveguide discharge, it is first necessary to briefly review and discuss the molecular spectra and the excitation processes of the gases involved. More detailed discussions of this subject is found in [7,8].

MOLECULAR SPECTRA

The lasing transitions of the CO₂ laser depend ultimately on the electronic, vibrational and rotational states of the linear triatomic CO₂ molecule. In this study of the CO₂ laser, we are mainly interested in the CO₂ and N₂ molecules and their interactions, due to the near-perfect match of CO₂(001) and N₂(v=1)

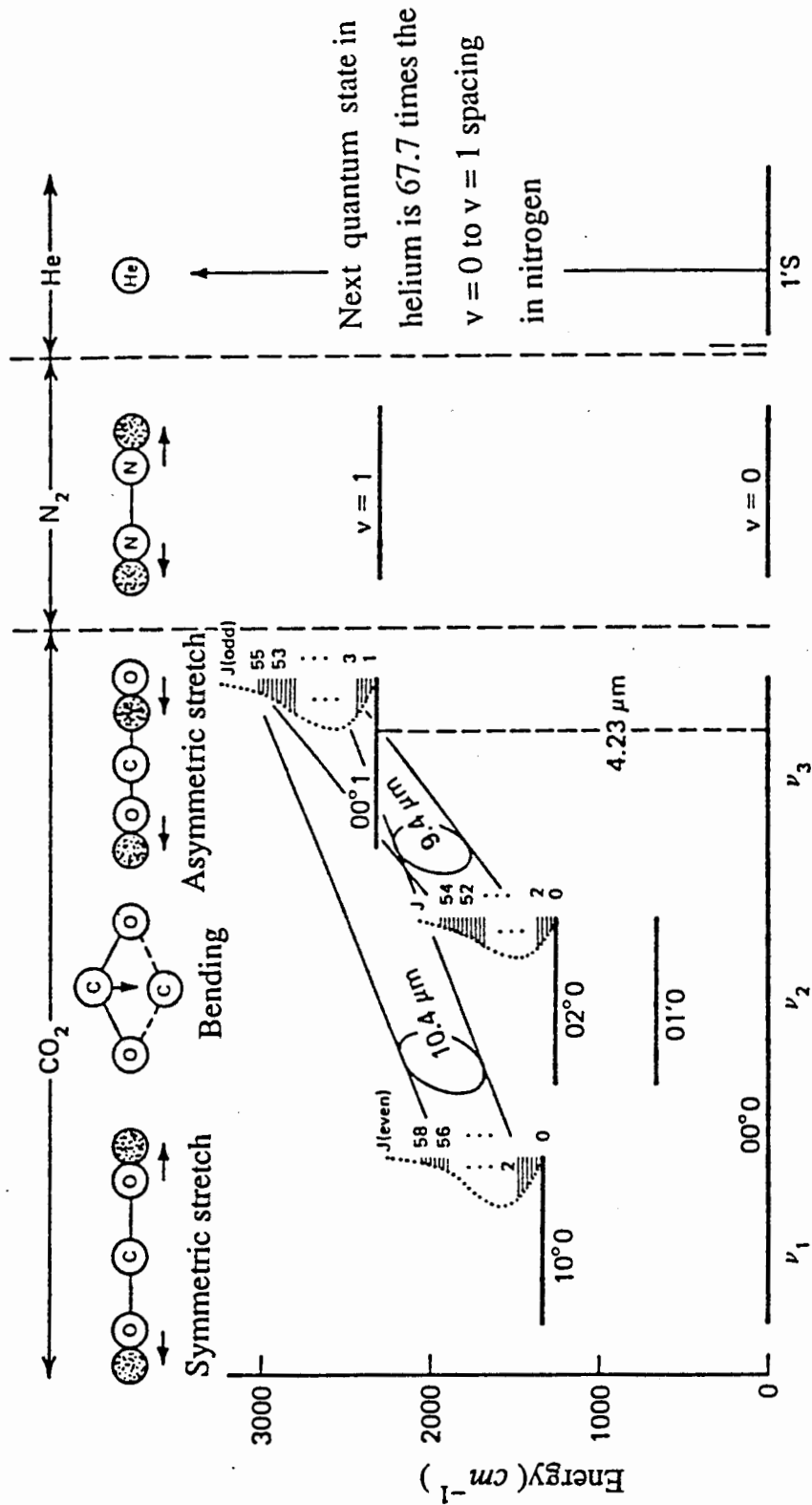


Figure 2-1-1. Energy level diagram of the $\text{CO}_2 : \text{N}_2 : \text{He}$ laser (ref.[11])

levels. The low-lying vibrational levels in the ground electronic states of CO_2 , N_2 and He are shown in fig. 2-1.

CO_2 Normal Vibrational Modes

The CO_2 molecule is a linear symmetrical molecule which has an internuclear axis and a plane of symmetry perpendicular to the internuclear axis. Since CO_2 is a triatomic molecule, it can execute three basic internal vibrations. These vibrations are called the normal modes of vibration, ν_1 , ν_2 and ν_3 , and they are [7,12]:

- a. *Symmetric stretch mode* (100, 200, etc.): In this mode, the oxygen atoms vibrate symmetrically along the inter nuclear axis. The energy spacing between these levels is 0.17 eV.
- b. *Bending mode* (010, 020, etc.): The atoms move symmetrically along an axis perpendicular to the internuclear axis. The energy spacing between these levels is 0.08 eV.
- c. *Asymmetric stretch mode* (001, 002, etc.): In this mode the atoms move asymmetrically along the internuclear axis. The energy spacing between these levels is 0.29 eV.

Therefore the state of the CO_2 molecule is described by three integers (ν_1 , ν_2 , ν_3) which represent the number of vibrational quanta of each mode. Equations 2.1 through 2-7 is taken from refrence [9]. The frequencies of the three vibrational modes were found by consideration of the valence force, to be

$$\omega_1^2 = \frac{k_1}{M_o} \quad (2.1)$$

$$\omega_2^2 = \left[1 + \frac{2M_o}{M_c} \right] \frac{2k_2}{M_o l^2} \quad (2.2)$$

$$\omega_3^2 = \left[1 + \frac{2M_o}{M_c} \right] \frac{k_1}{M_o} \quad (2.3)$$

where the valence force constants k_1 and k_2/l^2 have units of dyn/cm, M_o and M_c are the masses of the oxygen and carbon atoms respectively, and l is the inter-nuclear distance between them. These constants are given in [7, p.119]. The quantized energy levels can be calculated from the energy of a harmonic oscillator

$$E_i = h\omega_i (n_i + 1/2) \quad (2.4)$$

where $n_i = 0, 1, 2, \dots$

CO₂ Vibrational-Rotational Spectra

In addition to the vibration of the oxygen and carbon atoms with respect to one another, the CO₂ molecule is free to rotate. the energy levels of the rotational modes are given by

$$E_r = hcBJ (J + 1) \quad (2.5)$$

where J is the rotational quantum number and B is a rotational constant ($B = .387 \text{ cm}^{-1}$ at 400° k). The total energy of the CO₂ molecule can be approximated by adding the vibrational and rotational energies given by the equations (2.4) and (2.5). The rotational levels are very closely spaced. The population of the rotational level N_j with respect to the total population N_t is given by the Boltzmann distribution

$$N_j = N_t (2J + 1) \left[\frac{hcB}{kT} \right] \exp \left[\frac{-E_r}{kT} \right] \quad (2.6)$$

From eq.(2.6) the maximum population is found to exist in the rotational quantum level J_m which is equal to

$$J_m = \left[\frac{kT}{2hcB} \right]^{1/2} \quad (2.7)$$

where $J_m = 19$ at $T = 400^\circ \text{K}$ or $J_m = 29$ at 1000°K . Since the CO_2 molecule has no permanent dipole moment, radiation transitions between rotational levels in the same vibrational state are forbidden.

Over 200 oscillating CO_2 laser lines have been reported, resulting from the vibrational-rotational transitions and covering the spectral range from 9 to 18 μm . The strongest emission lines, occur in the 001-100 and 001-020 bands, at wavelengths of about 10.4 and 9.4 μm respectively.

Each vibrational state is labeled with a symbol giving the symmetry as shown in fig. 2-2 for CO_2 molecule. Two of these symbols are Σ_g for symmetric state (even J) and Σ_u for antisymmetric state (odd J). Because of this symmetry, odd rotational levels of the g type state such as Σ_g and even-rotational levels of the u type states such as Σ_u and Π_u are missing. The vibrational levels denoted with Π , Δ , etc., have two sub levels, positive and negative, for each value of J at slightly different energies, whose signs alternate $+-, -+, +-, \dots$ or $-+, +-, -+, \dots$. These sublevels are the result of the equivalence of two directions of the angular momentum l . The selection rules for the vibrational-rotational transitions are as follows [10]

vibrational transitions: $\Delta v = 1, \Delta l = 0, \pm 1, g \rightarrow u, u \rightarrow g$

rotational transitions: $\Delta J = 1, \pm 1, + \leftrightarrow -, s \leftrightarrow a$

where $+$ and $-$ represent even and odd J respectively, s and a represent the symmetric and antisymmetric eigenfunctions respectively. Laser action has been obtained from the P branch ($\Delta J = -1$) and the R branch ($\Delta J = +1$) of each band, the strongest lines are P(20) and R(20) which correspond to the two wavelengths 10.4 and 9.4 μm respectively. The Q branch ($\Delta J = 0$) is prohibited

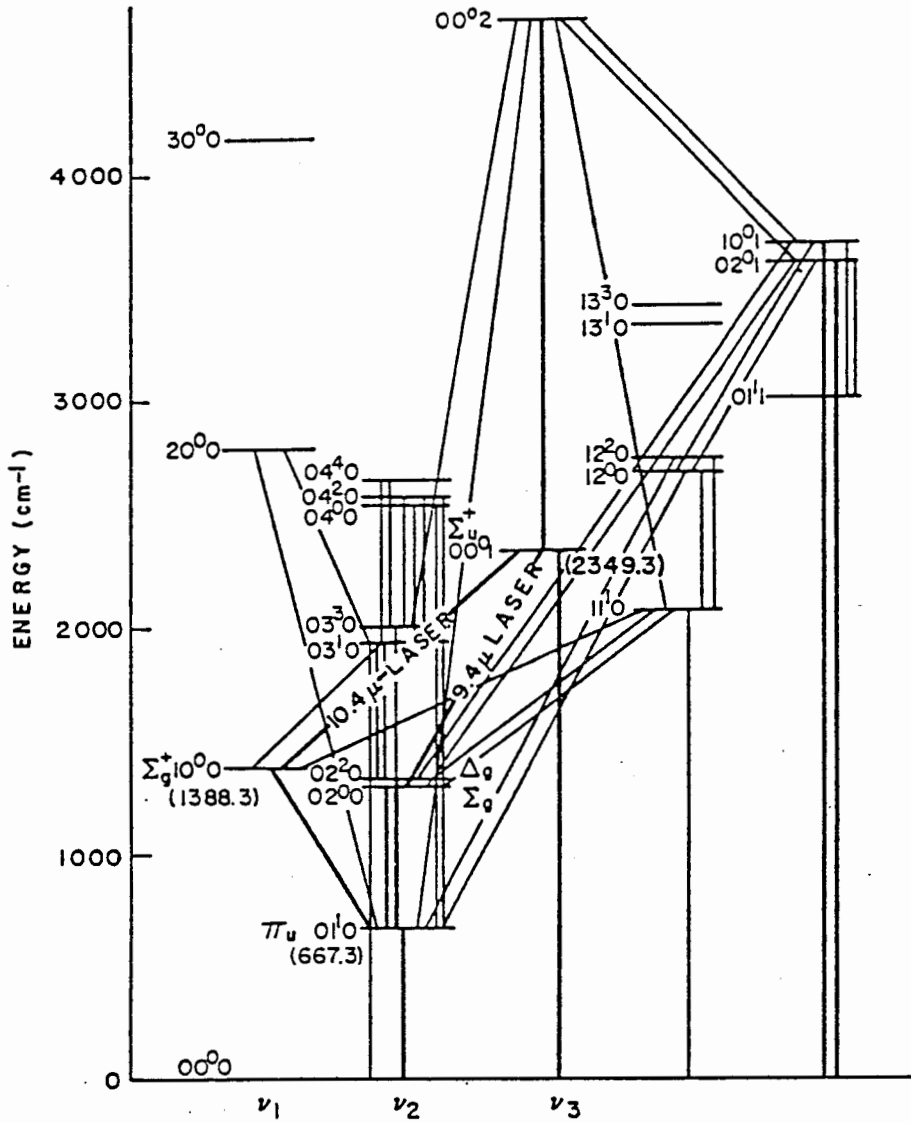


Figure 2-2. Energy level diagram of the CO₂ molecule (ref.[9])

because such a transition would occur between two Σ states of zero angular momentum.

Vibrational energy levels of Nitrogen

Since, nitrogen is a homonuclear diatomic molecule, it has only one degree of vibration. The lower vibrational levels of N_2 , from $v=1$ to 8 are spaced to have an excellent match with (000) to (001) separation of CO_2 , therefore, these levels can be used to efficiently populate the upper laser level of CO_2 . The nitrogen molecule has no permanent dipole moment in the ground electronic state, so the only way that these excited vibrational levels can decay in a discharge is through nonradiative collisions with other species. As a result, the vibrationally excited levels of nitrogen have a finite but very long effective lifetime of about 100 ms [7].

Helium

Helium is the dominant species in most CO_2 laser mixtures. Also, He has the highest ionization potential. The lowest electronic level in He occurs at an energy level of 19.7 eV. The beneficial role that He plays in a CO_2 laser discharge is to cool the gas by aiding in the depopulation of the lower laser level. He also plays a very important role in maintaining the energy distribution of electrons in the proper range [9,38].

EXCITATION PROCESSES

The two most important processes that populate the (001) upper laser level are: (1) direct electron impact, and (2) resonant transfer of energy between vibrationally excited N_2 ($v=1-8$) and ground state CO_2 (000).

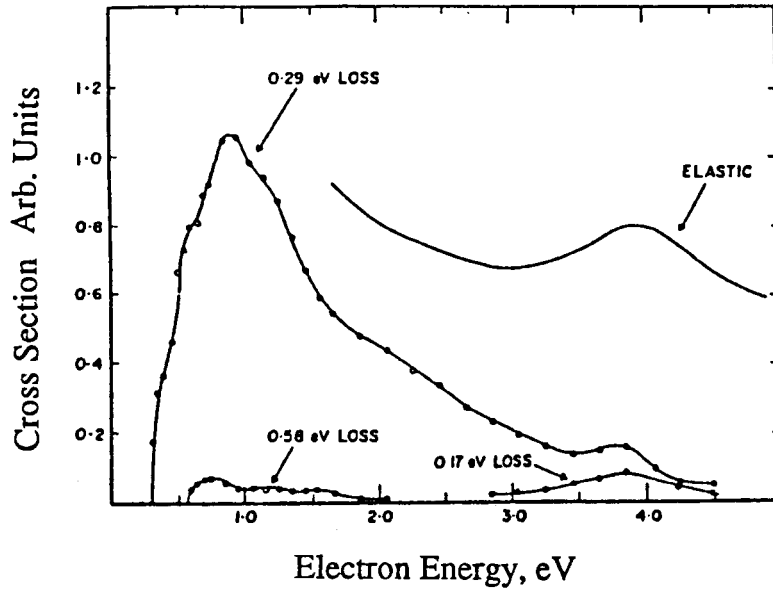


Figure 2-3. Energy dependence of elastic and inelastic cross sections in CO₂ (ref.[12])

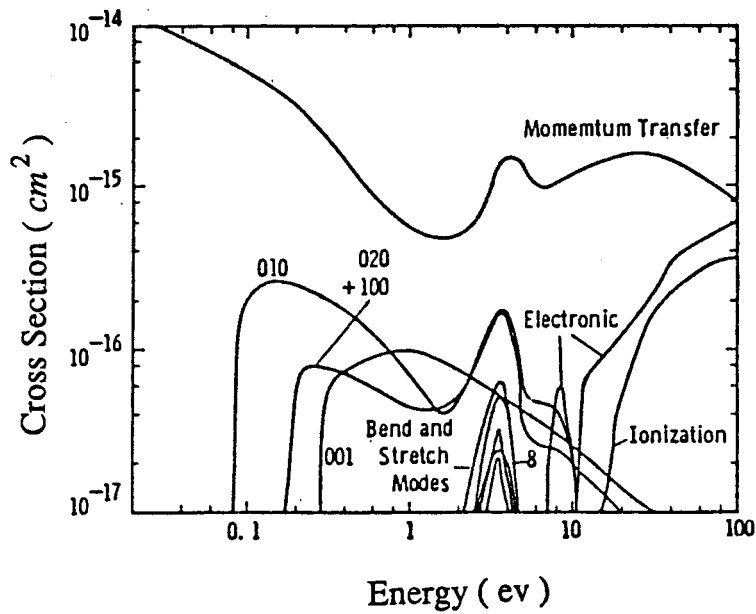


Figure 2-4. Momentum transfer and inelastic cross sections for electrons in CO₂ derived from electron transport coefficients (ref.[38])

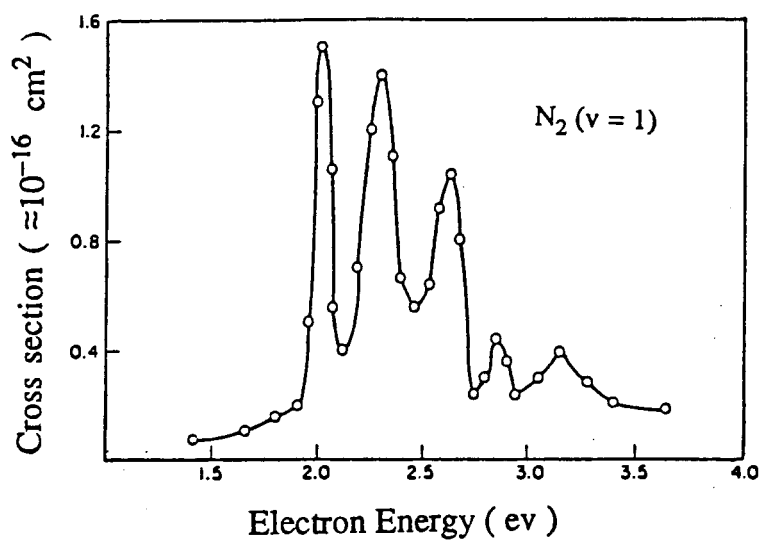


Figure 2-5. Cross section for vibrational excitation of N_2 ($v = 1$) by electron impact (ref.[13])

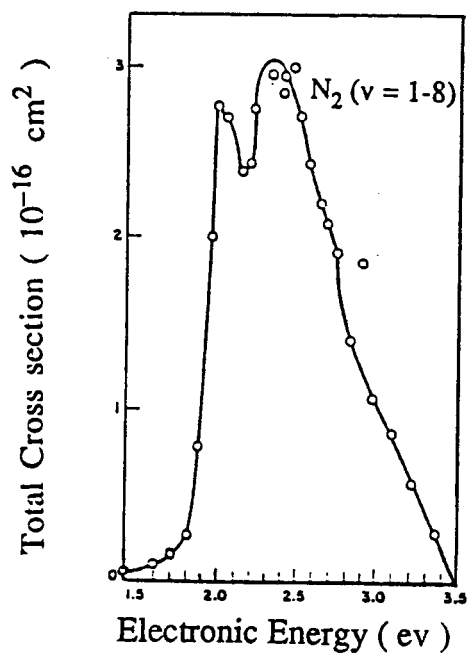


Figure 2-6. Total effective Cross section for vibrational excitation of N_2 ($v = 1-8$) by electron impact (ref.[13])

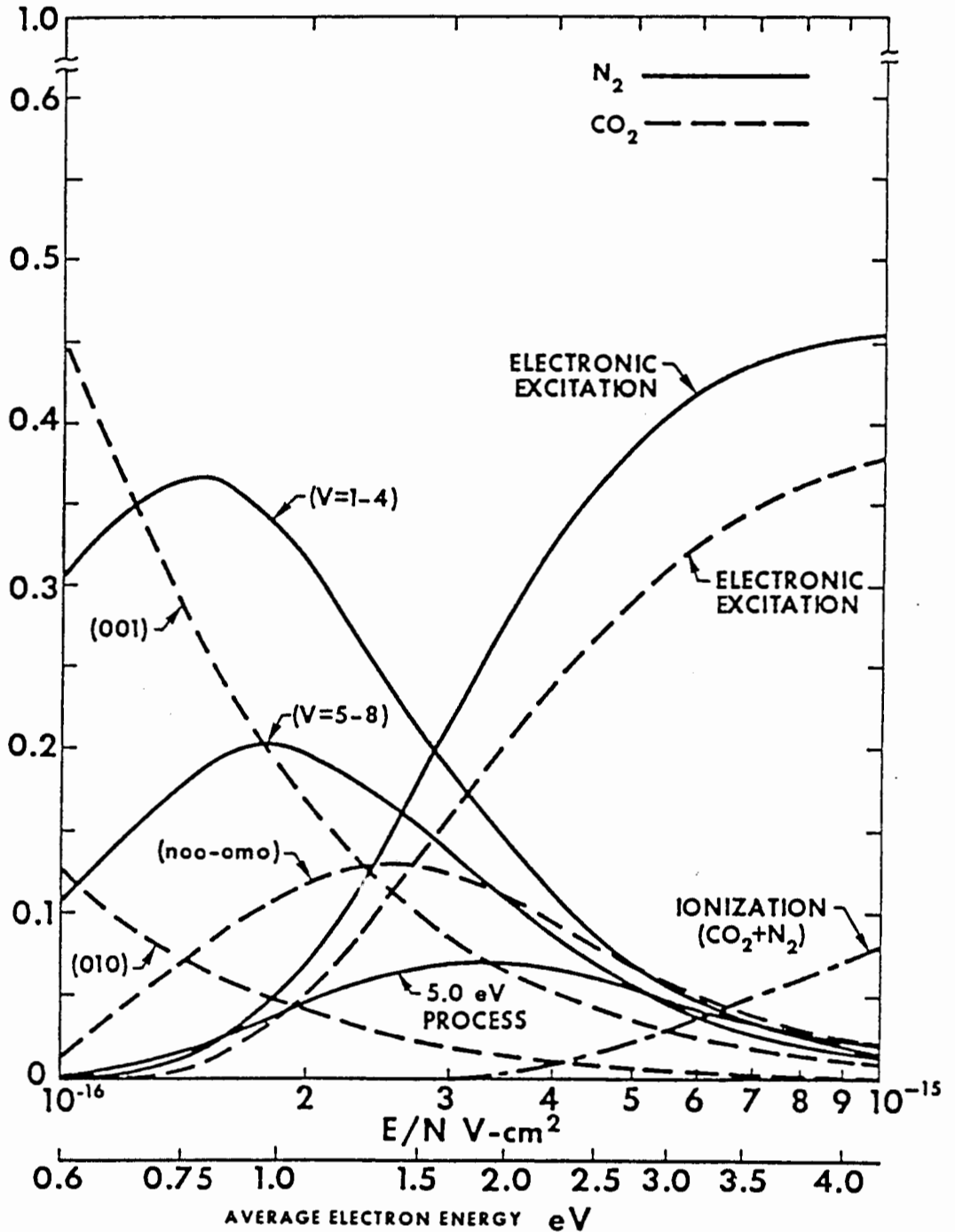
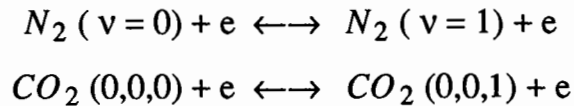


Figure 2-7. Fraction of power transferred from the electrons in a $\text{CO}_2:\text{N}_2:\text{He}$ (1:1:8) gas mixture discharge to CO_2 and N_2 as a function of E/N (ref.[16])

Direct electron impact

To understand this process, it is important to study the dependence of the vibrational-rotational cross-sections of CO_2 and N_2 on the energies of the electrons that collide inelastically with either a CO_2 or N_2 molecules. This type of collisions is called a collision of the first kind:



We will be mainly concerned with low energy electrons of 0-4 eV typical a CO_2 laser discharges.

As shown in fig. 2-3, the vibrational excitation of the upper laser level (001) of CO_2 by electron impact exhibits a peak collision cross section (probability of collisions) of about $3 \times 10^{-16} \text{ cm}^2$ at 0.9 eV, while the (002) excitation is an order of magnitude lower [12]. But as shown in fig. 2-4, Lowke et al. [38] found that the (001) cross section of Boness and Schulz [12] is about a factor of 3 too large to give consistent transport coefficients (i.e. electron drift velocity, ionization and attachment coefficients). From figs. 2-3,4, we see that the peaks of of the vibrational excitation cross-section (resonances) occur very close to the threshold for the onset of each energy loss process. Thus, the direct electron impact excitation of CO_2 is inefficient because levels other than the upper laser level will get populated for electron energy greater than .3 eV.

This is quite different from the situation observed in diatomic gases such as N_2 where the peak cross section occurs at energies well above the threshold [7, p. 142] as shown in figs. 2-5,6 [13]. The cross section of N_2 , shown in fig. 2-6, reaches a maximum of about $3 \times 10^{-16} \text{ cm}^2$ at an electron energy of about 2.3 eV. The difference between the energy needed to excite the vibrational level and the

resonance energy 2.3 eV is attributed to the lowest shape resonance characteristic of the so called boomerang states [14], where the energetic electron orbits the N_2 molecule for a short time before exciting it into a vibrational state [11, p.284].

As a summary of the above discussion, at energies typical of a laser discharge, different vibrational and rotational level of CO_2 molecules get excited. But when N_2 is added, the excitation of the upper laser level is increased due to the near perfect match of vibrational levels of N_2 and the upper laser level of CO_2 . The large N_2 vibrational cross section at 2.3 eV also exerts a strong influence on the electron energy distribution function by preventing electrons from reaching energies greater than 2.3 eV [15]. For example, for the gas mixture $CO_2 : N_2 : He$ of 1:1:8 when the E/N (electric field / neutral particle density) is $1.5 \times 10^{-16} \text{ V. cm}^2$, which correspond to an average electron energy of 0.76 eV, the electron will experience difficulty in reaching energies greater than 2.5 eV [16].

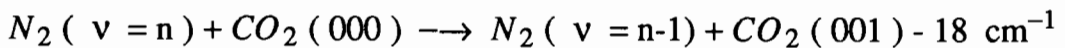
In general, the energy in a discharge is transferred from the applied electric field to the electrons, then from electrons to the neutrals that get excited by electron collision. This energy is lost by radiation and by metastable states that, under some conditions, transfer this excitation energy to other molecules. Fig. 2-7 shows the fractional power transferred from the electrons to N_2 and CO_2 molecules as a function of E/N and the average electron energy u . The calculation of fig. 2-7 was made for the gas mixture $CO_2 : N_2 : He$ of 1:1:8, but a change in gas mixture ratio did not change the fractional power transferred significantly. The E/N range $10^{-16} - 10^{-15} \text{ V. cm}^2$ is a transition region for this gas mixture in which the dominant electron energy transfer process changes from vibrational to electronic excitation [16]. The electronic excitation is of some importance in sustaining the

discharge. Therefore, it is important in a gas discharge to optimize the E/N value, so that the electron power transfer is divided between electronic and vibrational excitation.

At an average electron energy of 1 eV, typical of a CO₂ laser discharge, the fractional power transferred to the coupled CO₂ (001) - N₂ (v = n) system is about 70%. This percentage combined with the 41% quantum efficiency of the 10.6 μ m transition, suggests that a maximum efficiency of 30% is available from a CO₂ laser.

N₂ – CO₂ Resonance transfer

The selective excitation of CO₂ (001) from the ground state by N₂ (v =1) occurs at a very rapid rate of about $1.9 \times 10^4 \text{ torr}^{-1} \text{ sec}^{-1}$ [9]. The rapid rate is due to extremely low energy difference of ($\Delta E = 18 \text{ cm}^{-1}$) between N₂ (v = 1) and CO₂ (001), and also the long life time of the excited N₂ molecule. Therefore, the excitation of the CO₂ (000) level by N₂ (v = 1) level is through a collision of the second kind, which is given by



This reaction produces a mixed state in which the combined population of N₂ (v = 1) and CO₂ (001) are essentially in equilibrium. Due to this equilibrium, the efficiency of the CO₂ (001) level is increased by a factor of 2 upon the addition of even a few torrs of N₂ pressure [9].

From the above discussion and experimental observation, it is reasonable to expect the following: (1) The addition of He will stabilize the discharge and prevent arcing because the glow to arc transition usually occurs at lower value of E/N. To explain this, the average electron energy increases for the same E/N when the proportion of He is increased because He has none of the inelastic vibrational

losses that are present in CO_2 and N_2 . (2) The addition of N_2 will increase the output power and efficiency of the CO_2 laser due to the selective excitation of the upper laser level by excited N_2 .

CHAPTER III

LASER DISCHARGE

INTRODUCTION

The low pressure glow discharges have been studied qualitatively for almost a century and quantitatively for more than half a century. Unfortunately, some important properties of the glow discharge in the cathode region and in the striated positive column are still not quite understood. The glow discharge is discussed in detail in references [17,18,19].

The glow discharge is one of the most common pumping mechanisms in gas lasers, and the CO₂ lasers is no exception. Many different techniques and designs have been used to obtain an efficient discharge to establish a plasma for the required population inversion.

There are two main types of DC-discharge structures that have been used for CO₂ lasers . First, is the high-voltage, low-current longitudinal discharge which uses the positive column as the excitation medium [20]. Second, is the transverse-discharge which uses a closely spaced electrodes in order to minimize the high-voltage inherent in the longitudinal discharge [22,23]. The transverse discharge has a voltage-current dependence characteristic of an abnormal glow discharge which exhibits a positive impedance [22]. Thus, the high ballast resistor is no longer needed, and as a result, the transverse discharge is far more efficient than the longitudinal discharge. The main problem with the transverse discharge is the tendency to form arcing. This glow to arc transition at short electrode spacing

could be caused by the discharge sensitivity to pressure uniformity, surface cleanliness and electrode material. Other types of discharges such as coaxial discharges [23,24], hollow cathode discharges and in our case slotted hollow cathode (SHC) discharges could all be recognized as transverse discharges with different cathode shapes.

In this chapter we will first review the glow discharge and then the hollow cathode discharge and finally SHC discharge will be studied.

GLOW DISCHARGE

The voltage-current relation of a low pressure gaseous gap as shown in fig. 3-1, is the best general description of what will happen when an appropriate potential is applied across the electrodes. This relation illustrates that, after the ionization is initiated, the current grows with time and a distribution of electrons and positive ions fills the space between the electrodes. A further increase in current causes more ions to reach the cathode and eventually set up a space charge, distorting the field between the electrodes. At this point two effects are observed. First, the discharge exhibits visible light and dark spaces. Second, the potential across the electrodes drops considerably, resulting in a more efficient process. At this stage, when the properties of the discharge are first determined by space charges, a glow discharge is said to have been established [17].

A glow discharge is a silent luminous electrical discharge in which electrons are emitted from the cathode under the bombardment of particles and light quanta from the gas. A low pressure glow discharge consists of various regions of alternating dark and luminous zones. The actual location of these regions and the occurrence of a few of them depends upon pressure, current, electrode gap and

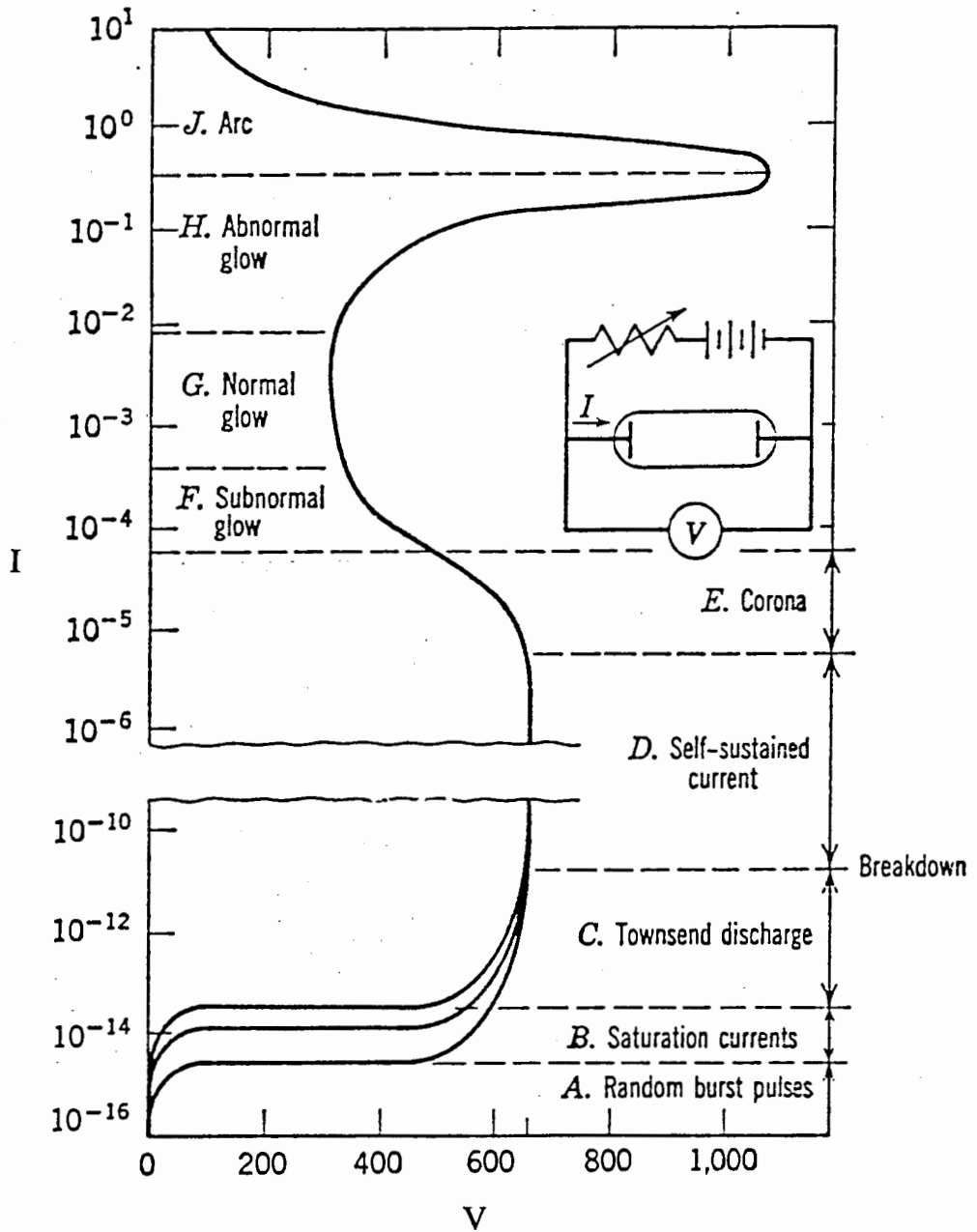


Figure 3-1. Voltage-current relation of low pressure gaseous gap (ref.[19])

type of gas used. A typical example is shown in fig. 3-2 for a normal discharge in a long cylindrical tube. Starting from the cathode, the glow discharge regions are Aston dark space, cathode glow and dark space, negative glow, Faraday dark space, positive column, and the anode dark space and glow. These regions could be explained as follow:

1. Aston dark space (ADS):

This region is very thin and completely dark. The emitted electrons, with energy of only a few eV, accumulate in this region to be accelerated through the cathode spaces. The electric field is highest in this region. ADS length decreases more strongly than cathode dark space length with increasing cathode fall V_c (the potential drop across the cathode including the Astone dark space).

2. Cathode glow and dark space:

The cathode glow is sharply defined due to the beam like properties of the electron stream. The electron energies rises rapidly with distance from cathode, and as a result some electrons produce excitation in the cathode glow region [17, p .60]. Electrons which lost their energies in excitation are accelerated again. In the cathode dark space, the electrons move too fast to produce any appreciable excitation, but they make some ionizing collisions and the electrons produced are also accelerated. Thus, the ionization increases with distance from the cathode, while the electric field decreases almost to zero at the boundary of the negative glow [17]. The potential drop V_c is a strong function of the gas used and the cathode material. From fig. 3-1, depending on V_c , there are three types of glow discharges as shown in fig. 3-1, they are as follow [17,19]:

(a). *subnormal glow*: When the current is so small that the discharge covers only

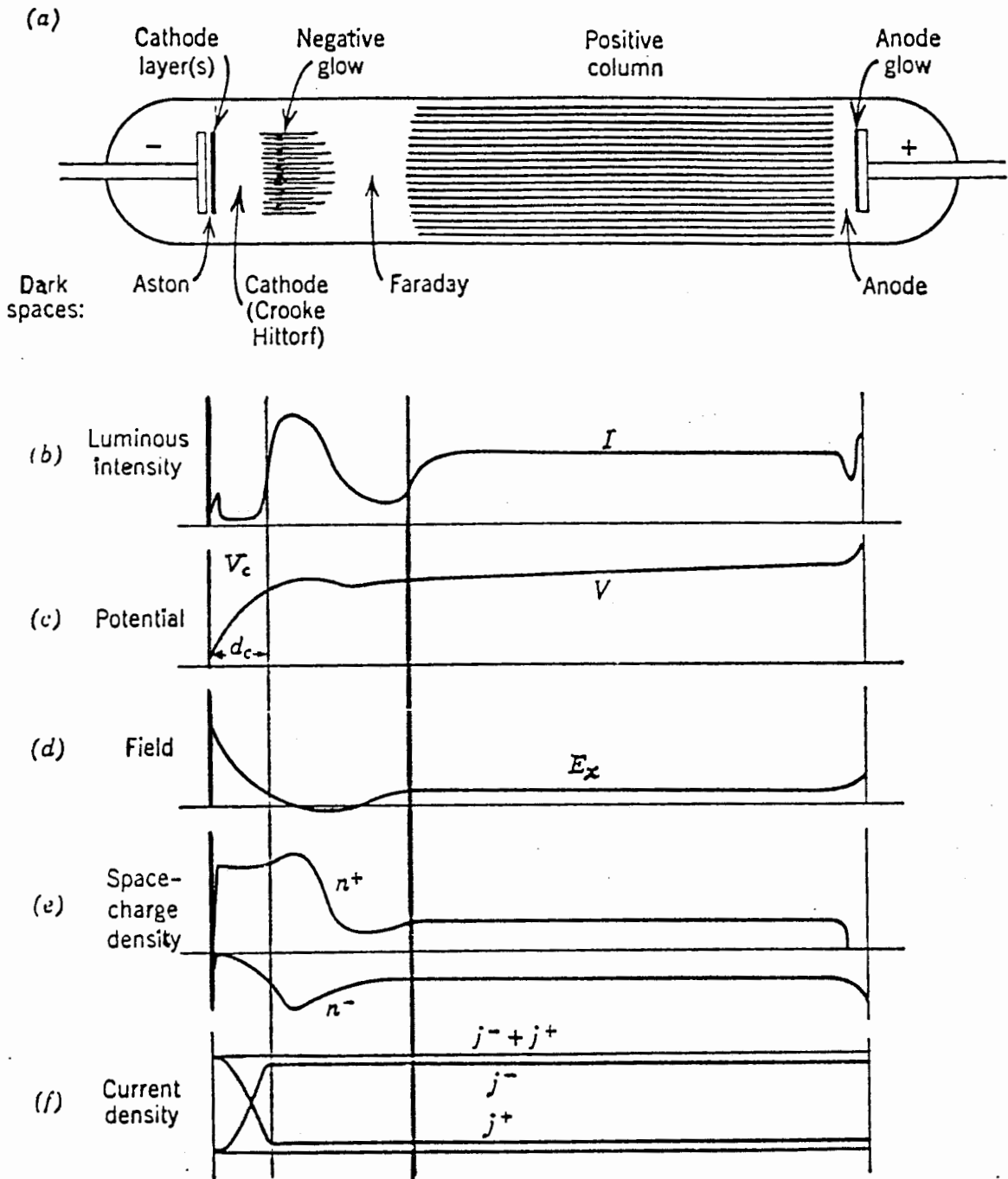


Figure 3-2. The normal glow discharge in neon in a 50 cm tube at 1 torr (ref.[19])

a very small part of the cathode surface. In this region V_c decreases with current.

- (b). *normal glow*: In this region the current density is constant. The area of the cathode covered by the discharge is proportional to the total current. In this region V_c is independent of current.
- (c). *abnormal glow*: In this region the negative glow covers the whole cathode and may be forced to occupy other auxiliary surfaces. As a result the electrode configuration, shape and material have a major influence on the plasma. An increase in current is obtained by an increase in current density which result in an increase in V_c . Therefore, the electric field increases at the cathode with the increase in current. With the increase in voltage the length of the cathode dark space decreases and the length of the negative glow increases slightly. In a strongly abnormal glow, the cathode can becomes very hot. Thus, it changes the pressure close to its surface and populates the lower laser level. Therefore, it is important to avoid this problem by cooling the cathode. Also in a strongly abnormal discharges, relatively little ionization occurs in the cathode dark space, but many ions flow from the negative glow [17]. Transverse laser discharges are usually operated in the abnormal glow region.

3. Negative glow (NG):

This is the brightest region in the glow discharge. Its color is characteristic of the gas. It is a field-free space where electron lose all or part of their energies. NG has a sharp boundary with the cathode dark space. A short distance from this boundary , the luminosity increases to a maximum then decreases slowly where the glow merges diffusely into Faraday dark space. This variation in brightness is

caused by two main groups of electrons crossing the boundary into the NG. One group consists of a large number of low-energy electron (slow) electrons produced by ionization in the cathode dark space. The other group consists of rather fewer high-energy (fast) electrons coming straight from the cathode and having almost the same energy as the cathode fall [17,p. 60]. The slow electrons produce the intense light at the cathode end of the glow. The fast electrons also suffer many inelastic collisions but penetrate further from the cathode. Therefore, the total light intensity in the glow rises to a maximum at which the largest collision cross sections are observed, and then diminishes toward the anode. In a discharge with almost normal or abnormal fall, there are three distinct groups of electrons in the middle of the NG having mean energies of about 25 eV, 7 eV and 0.5-2 eV [17,p. 111]. In a strongly abnormal glow, it appears that more fast electrons than slow electrons enter the glow due to less ionization in the cathode dark space. Toward the Faraday dark space, all beam like properties of the electrons are lost due to inelastic collision they suffered. Therefore, they become slow and their motions become quite random. The length of the NG is proportional to V_c/P .

4. Faraday dark space (FDS):

This region is relatively dark due to the low energy electrons that leave the NG. The boundary with the NG is quite vague because of the random motions of electrons. Due to an excess of electrons at this boundary, a net negative space charge is developed. At this point, the electric field rises slowly and extends toward the anode.

In the transition region from NG to FDS, direct excitation becomes less compared to collisions of the second kind. Since electrons in the FDS have energies (less than 1 eV), it has been suggested that only collisions of the second kind

occur [17,p. 112]. Finally, the length of the FDS has been shown to increase with the radius of the discharge tube, and it is usually longer than the NG.

5. Positive column:

The positive column is the most studied region of the glow, therefore, only important characteristics are mentioned. This region is the luminous part of the discharge between the FDS and the anode dark space. The color of the positive column is a characteristic of the gas which is different from that of the NG. It is also less bright than the NG. Photoemission stems from the excited and ionized molecules. The gas in this region is in the ionized state with equal density of positive and negative particles. The current in the positive column is mainly carried by electrons because of the small mobility drift velocity of the positive ions.

6. The anode dark space and glow:

The anode in a glow discharge acts as a collector of electrons which strike its surface. The properties of the anode region are dependent on the location of the anode[17].

When the anode is in contact with the positive column, a space charge buildup will be found on the surface of the anode. Compared to the positive column, the electric field in the anode region is greater and the potential drop is more positive. As a result, the positive ions are created in this region to flow into the positive column. Ion creation could be explained in the following processes. First, the electrons emerging from the positive column are too slow to excite, producing a very thin dark space. While in this dark space, these electrons gain from the electric field enough energy to ionize and hence produce a layer of light close to the anode surface due to excitation which called the **anode glow**. That is why

the anode fall is found usually to be of the same order as the ionization potential. It has also been shown that this potential increases with current density.

The other location of the anode is when the anode is placed in the FDS close to the NG. In this region a considerable number of electrons diffuse to the dark space. If sufficient electrons diffuse to the anode, then there will be no anodefall or glow. In this case the electric field, up to the anode surface, is almost the same as it would be in the undisturbed dark space.

Finally, there must be a transition between the above two regions. At a critical distance from the cathode, the anode fall develops suddenly. It is located at the anode end of the FDS. This distance is large at low pressure which aids diffusion, and also large when the cathode fall is large since it causes the primary electrons to have a greater range and length than the NG. An attempt to explain theoretically the behavior of the electric field in the FDS is presented by Ahsmann [33]. In this study he concluded that when increasing the distance between the anode and the NG, the reversed field strength becomes zero; only then rather suddenly an anode fall develops.

HOLLOW-CATHODE GLOW DISCHARGE

A hollow cathode discharge (HCD) could be achieved when the pressure is low and the cathode is two parallel-plane surface or a hollow cylinder. As an example, consider two plane cathodes facing each other as shown in fig. 3-3a, that are separated by a relatively large distance x_c . Each cathode will be covered by a cathode dark space (CDS) and a NG. The direction of the velocities of the high-energy electrons, that cross from the CDS into the NG, will be towards the opposite cathode. There, these electrons will lose energy due to collisions and finally

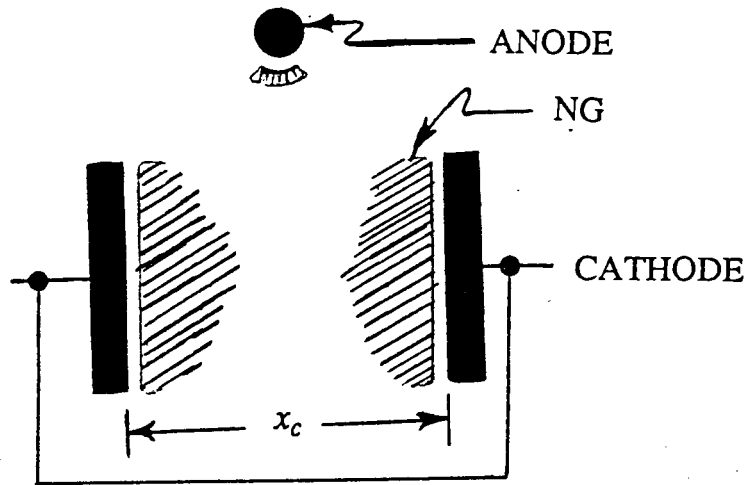


Figure 3-3a. Parallel-plane cathode discharge system configuration

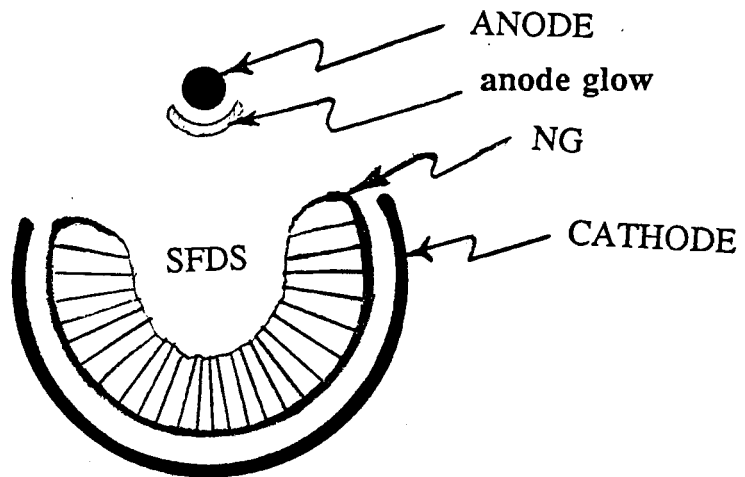


Figure 3-3b. Slotted hollow cathode discharge system configuration

reverse their directions in the CDS. As a result, the energy of the electrons moving towards the anode is reduced due to their high collision rate in the cathode regions [26]. As x_c is reduced, the mean random velocity of the electrons in the FDS is reduced. As x_c is further reduced, the density of the high energy electrons increases especially when the two NG's merge. This causes more efficient positive ion production and higher current density for the same cathode fall. Therefore, HCD is usually used to form a strong NG by the superposition of two NG's opposite to each other. Usually, a cylindrical hollow cathode is used because it forms a stronger NG.

From the above discussion, we could say that the main properties of HCD, which depends strongly on the tube diameter, are a current density orders of magnitude higher than that of a plane cathode discharge (PCD) and the extreme brightness due to the confinement of the NG. HCD has been used to excite high-lying atomic and ionic levels such as noble gas (e.g. He) and noble gas metal mixtures (e.g. He-Cd). The creation processes of high-energy electrons are as follow [29]:

1. Secondary emission of electrons on the cathode due to ions, ultraviolet photons and to a small extent metastable atoms.
2. Ionization in the CDS.
3. The high-energy electrons that cross the NG to the opposite CDS where they are decelerated and reverse their direction in the CDS.

And the loss processes of high-energy electrons are as follow:

1. Inelastic collisions in the NG where the electric field is very small.
2. The unavoidable leakage of some electrons that escape the trap formed by the HCD.

Different designs of hollow cathode (HC) are discussed in ref. [28]. There are two basic groups of HC designs, depending on the direction of the electric field with respect to the cathode axis. One group is called transverse HC and the other is called longitudinal HC. We will be mainly concerned with the transverse HC. Various types of HCD's have been used as a gain media for He-Ne lasers [30], He–Cd⁺ lasers [31], argon ion lasers and other high-lying ionic level lasers. A single-pass gain of 10 percent per meter have been reported in the NG of HCD in CO₂–He mixture [25].

Recently, a longitudinal CO₂ laser operating at 400 V from a three phase line with HCD has been reported [32]. Output laser pulses of 2 ms FWHM, 3 W peak power and a repetition frequency of 100 MHz were obtained from this laser.

From the above discussion and experimental measurements, we conclude that using the NG of HCD as an excitation media for CO₂ laser is not very practical because of the low gain achieved. This low gain could be explained by the fact that the NG plasmas have a very high concentration of low-energy electrons below 3 eV and a positive ions produced by the high-energy electrons above 20 eV. These characteristics provide a high recombination rate which lower the gain of the CO₂ laser [25].

Theory of HCD

A complete theoretical treatment of HCD has not yet been achieved. Most of the theories written up to now are of a He discharge and use the cathode fall theory. The qualitative theory of HCD such as the effect of cathode separation x_c and the anode-cathode separation on the HCD, is presented in ref. [26]. The quantitative theories are presented in ref. [27-29].

The theory presented here is based on the improved cathode fall theory developed in ref, [28]. There are two important parameters in HCD that we are trying to solve for, the thickness of the CDS and the other is the current density. They are usually expressed in terms of Pd and $\frac{J}{P^2}$ respectively, where P is the pressure, d is the thickness of the CDS and J is the total current density. According to Fujii et.al. [28], the electron multiplication factor is given by:

$$M = (1 + 1/\gamma) (1 - \delta) \quad (3.1)$$

where γ is the number of secondary electrons per ion striking the cathode, and δ is the coefficient of ion current density diffused into the CDS from the NG. The ratio of the total current density to ion current density at the cathode is

$$\eta = \frac{J}{(J_+ + \delta J)} \quad (3.2)$$

therefore

$$J = \eta (J_+ + \delta J) = \eta \rho v_+ = \eta \frac{E}{4\pi d} v_+ \quad (3.3)$$

where J_+ is the ion current density formed in the CDS, ρ is the density of the space charge. And the drift velocity of the positive ions falling on the cathode surface is

$$v_+ = \mu^+ \frac{E_k}{P} \quad (3.4)$$

where μ^+ is the positive ion mobility, and E_k is the electric field at the cathode surface. From eq. (3.3) we obtain

$$J = \eta \frac{\mu^+ E_k^2}{4\pi(Pd)} \quad (3.5)$$

substituting the relation $E_k = \frac{2V_k}{d}$ in the above equation, where V_k is the cathode

fall potential, we get

$$\frac{J}{P^2} = \eta \frac{\mu^+}{P} \frac{V_k^2}{(Pd)^3} \quad (3.6)$$

where $Pd = \frac{1.25}{A_1} \ln M$. A_1 is a constant that depends on the kind of gas. From this result, it is clear that the current density decreases with increasing values of Pd .

SLOTTED HOLLOW-CATHODE DISCHARGE

The discharge of the our waveguide is a transverse discharge of a slotted hollow-cathode (SHC). Fig. 3-3b illustrates the cross-section configuration of this SHC discharge. This type of configuration has some of the HCD advantages and the favorable effect of the slot along the HC. These advantages could be summarized as follow: (1) rigid and high thermal conductivity metal cavity, (2) low discharge voltage, (3) low positive impedance similar to the abnormal glow of plane cathode, (4) homogeneity of the discharge along the cathode center (optical axis), and (5) the slot along the cathode provides a path for the electric field to penetrate into the hollow-cathode cavity, provided that, at the appropriate discharge conditions for laser gain, the width of the slot is not closed by the opposite NG's. This last point could be explained in the following paragraph.

For lower values of J/P^2 than that used in regular HC operations, when the distance between the opposite NG's is relatively large, a potential difference V_g exists between the edges of the NG close and remote from the anode. As either the P increased or J decreased, the conductivity will decrease due to a decrease in electron collision frequency and charged-partical density respectively. The thickness of the NG will also decreases with decreasing J/P^2 . Thus, the conductivity

of the NG decreases and the value of V_g necessary to maintain a given current will increase. As a result, when the distance between the opposite cathode surfaces is reduced, so that the electric field penetration in the cavity is reduced and a greater proportion of the total current consequently flows transversely through the glow, an appreciable rise in V_g will result if J/P^2 is small. Therefore, for lower values of J/P^2 compared to values used in HC, the slot serves to provide a path for the electric field to penetrate into the HC cavity and as a result to reduce V_g . This is favorable in our case because very high V_g causes the electrons to have higher energies than needed for efficient excitation of the upper CO_2 laser level.

In our work, we will use the region between the opposite NG's. Since this region is dark and occurs after the NG, we will call it the special FDS or SFDS. This SFDS is formed in the middle of the cathode cross-section and serves as the laser gain medium for three reasons: First, the NG is not a practical plasma for the excitation of the upper CO_2 laser level. Second, the positive column is hard to obtain inside the HC. Thirdly, from the above paragraph, it is possible to get the optimum electron energy for excitation of the upper CO_2 laser level. Obtaining this SFDS in the middle of the cathode cross-section is done by adjusting the gas pressure, mixture ratio of ($\text{CO}_2 : \text{N}_2 : \text{He}$) and current. And by using a relatively large diameter where in our case ($\text{ID} = 1.1 \text{ cm}$). As a result, the NG will form a C-shape close to the cathode surface with a thickness of about 2 mm for the above diameter and this thickness changes depending on the discharge parameter. From visual observation, the anode glow was always found to exist at the attainable pressure range (6-15 torr), while no positive column was observed.

This SFDS is unique because of the focusing effect of the SHC configuration

compared to a plane-cathode and is the effect of the slot along the cathode compared to HC structure. In this SFDS, the CO_2 laser gain was found to be comparable to the gain in the regular longitudinal positive column plasma for the same gas pressure, mixture ratio and flow rate. Fig. 3-4 shows the V-I characteristics exhibited by the transverse SHC discharge for different gas mixtures. The positive impedance exhibited by the discharge is similar to the abnormal glow impedance except in SHC discharge we get more current for the same voltage.

Since no direct measurements of the actual electric field E or electron temperature T were taken during this work, I will try to give a very rough numerical estimate of some of the discharge parameters in this region. A very good estimate to start, is to assume the potential drop across the CDS to be 340 V and the potential drop across the anode spaces to be 20 V. This makes the potential drop across the SFDS to be 30 V when the potential drop across the electrodes is 390 V. The length of the SFDS from the end of the NG to the anode glow is approximately 6 mm. From the above estimates and the assumption that the electric field E is linear in the SFDS, E will be 50 V/cm. Therefore, the E/N (the ratio of the E-field to neutral particle density) is 1.57×10^{-16} V- cm^2 for a pressure of 9 torr. Using this result in fig. 2-7, the average electron energy is approximately .9 eV.

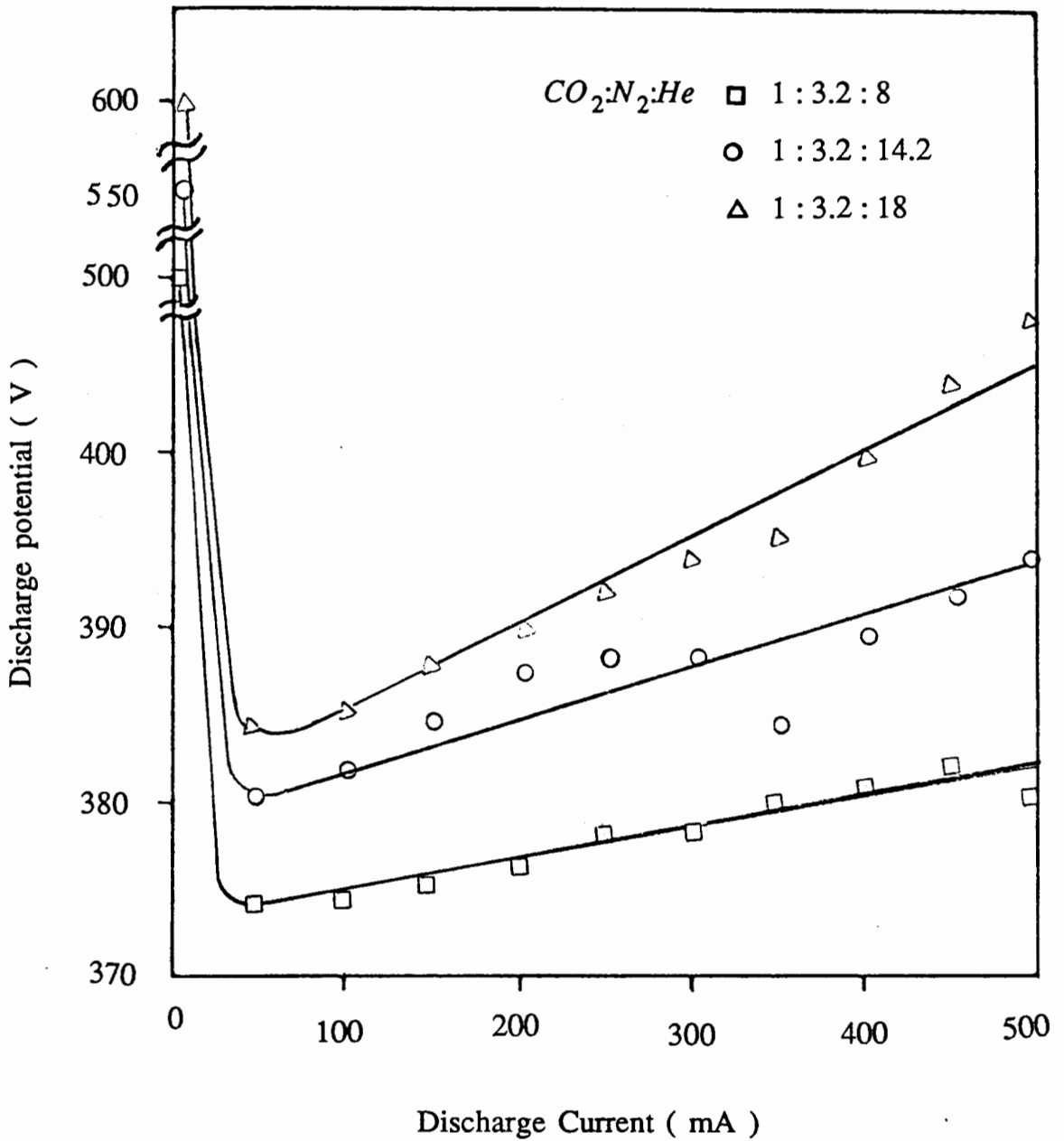


Figure 3-4. Voltage-current characteristics of the waveguide discharge for different gas mixtures

CHAPTER IV

GAIN MEASUREMENT

INTRODUCTION

Gain measurement is a necessary step to assess the suitability of this waveguide discharge for laser excitation, to perform a comparison of this waveguide configuration with existing schemes and finally to obtain the optimum condition for laser action. Single-pass gain measurements have been performed as a function of gas mixture ratio, pressure, current and radial distance from cathode. Other measurements such as gain as a function of E/P and gas temperature were not performed, but they were substituted by repeating the above measurements many times to get the optimum conditions for laser gain. These measurements have been made in the active medium of the discharge containing CO₂, N₂ and He.

The gain represents the fractional increase in intensity per unit length of laser medium. This gain is equal to the product of the stimulated emission cross-section and inverted population difference. In the case of 10.6 μm CO₂ laser, this population difference is mostly between the two vibrational levels (001) and (100). Finally, the gain increases with decreasing gas temperature since an increase in gas temperature results in the increase of the lower laser level and a decrease in the stimulated emission cross-section.

THEORY

The amplification of a small-signal passing through an inverted laser medium is described by the rate equation for intensity [34]

$$\frac{\partial I}{\partial z} + \frac{n_o}{c} \frac{\partial I}{\partial t} = (g(\nu, I) - \gamma)I \quad (4.1)$$

where I is the intensity inside the active medium, $g(\nu, I)$ is the intensity and frequency dependent gain coefficient and γ is the loss coefficient. For a steady state low loss amplifier, equation (4.1) can be written as

$$\frac{dI}{dz} = g(\nu, I)I \quad (4.2)$$

At this point, we have to discuss briefly the various line broadenings mechanisms and the corresponding behavior of $g(\nu, I)$. The major types of line broadenings are homogeneous and inhomogeneous line broadening. These two broadenings differ from each other by their saturation behavior.

Homogeneous Broadening

This type of broadening occurs in a system when the atoms or molecules are identical. This means that each molecule in this collection of molecules has the same center frequency and the same frequency response. When a signal is applied to this collection, it will have the same effect on all the atoms.

The most common homogeneous line broadening mechanisms are:

1. Phase interrupting collisions with phonons, collisions of like atoms (Lorentz) or collisions of unlike atoms (Holtsmark).
2. Finite lifetime of laser levels due to spontaneous emission (natural broadening)

The line shape of these two mechanisms is Lorentzian; and the gain saturation is given by

$$g(\nu, I) = \frac{g_o}{1 + \left[\frac{2(\nu - \nu_o)}{\Delta\nu_h} \right]^2 + sI} \quad (4.3)$$

where g_o is the unsaturated line center gain, and s is the saturation parameter ($1/I_s$), where I_s is the saturation intensity, and $\Delta\nu_h$ is the homogeneous line width ($\Delta\nu_h = 100$ MHz [37]).

Inhomogeneous Broadening

Inhomogeneous line broadening occurs when the atoms in a system are different. This means that different atoms or groups of atoms within the same collection have slightly different resonance frequencies. Therefore, the response of this collection is broadened in frequency.

The most common inhomogeneous line broadening mechanisms are:

1. Doppler broadening which is typical of gases due to the atomic motion.
2. Local inhomogeneities of the electric field in a solid due to lattice imperfections which causes local variation of the energy levels of the atoms (Stark effect).

Inhomogeneous line broadening often has a Gaussian line shape; and in such case the gain is given by

$$g(\nu, I) = \frac{g_o e^{-\left[\frac{2(\nu - \nu_o)}{\Delta\nu_d} \right]^2 \ln 2}}{\sqrt{1 + sI}} \quad (4.4)$$

Where $\Delta\nu_d$ is the doppler line width. Comparing eq.(4.4) to eq.(4.3), we see that

the inhomogeneous line shape saturates more slowly than the homogeneous line shape.

Since the operating pressures are all above 5.2 torr, the effect of Doppler broadening is small compared to collisional broadening [35,36]. Therefore, in deriving the small-signal gain equation, the inhomogeneous line broadening is ignored. The homogeneous line width is approximately 100 MHz [37].

Substituting equation(4.3) into equation(4.2) and assuming $I \ll I_s$, we get

$$\frac{dI}{dz} = g_o(\nu)I \quad (4.5)$$

to which the solution is given by

$$I(z) = I(0) e^{g_o(\nu)z} \quad (4.6)$$

then for a gain medium of length L the gain is given by

$$\begin{aligned} g_o(\nu) &= \frac{1}{L} \ln \frac{I(L)}{I(0)} \\ &= \frac{1}{L} \ln \frac{I_{on}}{I_{off}} \end{aligned} \quad (4.7)$$

where

I_{on} : intensity with discharge on

I_{off} : intensity with discharge off

GAIN MEASUREMENT APPARATUS

The gain measurements were performed using the apparatus illustrated in fig. 4-1. A conventional low power CO₂ laser was used to provide a low order TEM mode probe beam. The higher order modes were eliminated by an aperture. The probe beam laser has a 1-cm diameter, 150-cm long water cooled discharge tube with a Brewster window at each end. The discharge tube was placed between

a 2-m gold coated curved mirror and a flat germanium mirror with 80 percent reflectivity, forming a 185-cm long resonator. The discharge current was 15-25 mA at 5-8 kV. The gas mixture $\text{CO}_2 : \text{N}_2 : \text{He}$ of 1:1:8 was used at a pressure of 7-10 torr.

Since the probe beam is invisible, a He-Ne laser was used to show the probe beam path, as shown in fig. 4-1. The flat mirrors M_1 and M_2 provided the alignment of the He-Ne laser. The available beam splitter M_3 (80 % reflectivity at $10.6 \mu\text{m}$) served as the point where invisible $10.6 \mu\text{m}$ beam merged with the He-Ne beam. After this point, the two beams propagate collinearly. M_4 (max. reflectivity at $10.6 \mu\text{m}$) redirects the beam to M_5 (2-m curved mirror, max. ref. at $10.6 \mu\text{m}$) which focuses the beam at almost the center of the waveguide with a beam waist of 2 mm. The two mirrors M_5 and M_6 (M_6 is max. ref. at $10.6 \mu\text{m}$) provided the alignment of the two beams to propagate collinearly through the waveguide parallel to its axis.

The probe beam scanned across the amplifier perpendicular to the waveguide cross-section by translational movement of M_6 . Each one of the two salt windows s_1 and s_1 was mounted at one end of the amplifier. After passing through the amplifier, the probe beam is detected by a SCIENTECH 362 power meter. Equation(4.7) requires two sets of power measurements, when the discharge is on and off.

During these measurements, the low power probe beam did not exceed 0.3 watt. This means an intensity of 9.5 W/cm^2 , which is well below the reported saturation intensity 45-189 W/cm^2 [24,36]. A gas flow rate of approximately 1 SCHF was used during all gain measurements.

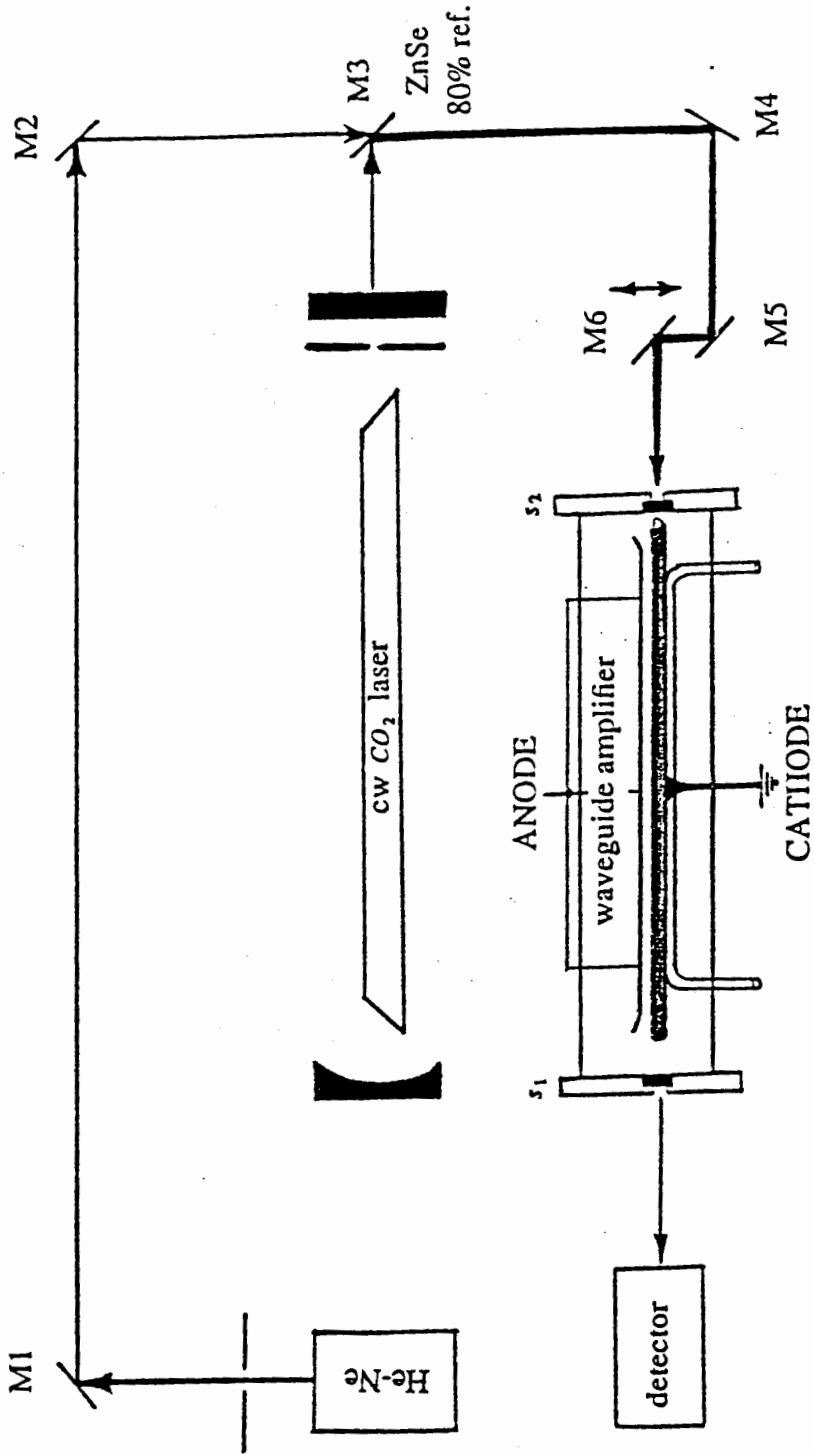


Figure 4-1. Gain measurements apparatus

RESULTS OF GAIN MEASUREMENTS

Starting with fresh gas, the gain measurements revealed a rapid drop in gain to just a little more than one third of its initial value within 2 min. Then the gain leveled off to a steady-state. This problem maybe caused by contamination of the gas. The structure which contain the waveguide is very large ($D = 9 \text{ cm}$) compared to the gain medium ($d = 1.1 \text{ cm}$); this causes a non uniform gas flow through the waveguide amplifying medium, and causes a contamination of the gas. Therefore, all the gain measurements were taken with fresh gas. Thus, these measurements were taken with further optimization in mind and do not necessary correspond to the device operation in this work.

Gain as a function of gas mixture ratio

Due to the instability of the discharge and arcing at lower ratios of He/ CO₂ , it was very hard to examine the gain when the ratio of He/ CO₂ is less than 8 without damaging the waveguide due to arcing. The optimum choice of gas mixture to have a stable discharge and a relatively high gain was at CO₂ : N₂ : He of 1:3.2:14.2. From fig. 4-2 and fig 4-3, the highest measured gain is a bout 140 percent for a mixture of 1:3.2:8 at a current 0.5 A. The gain increases as the ratio of He/ CO₂ decreases, and the gain is higher at higher current as shown in fig. 4-2. From fig. 4-3, the gain is highest when the ratio of N₂/CO₂ is 2-3.5. The sensitivity of the gain, to the N₂/CO₂ ratio, increases as He/ CO₂ ratio increases.

Gain as a function of pressure

The pressure difference between the inlet gas pressure after the flow meters P_i and the outlet at the pump P_o is very large; therefore, it is necessary to use the average pressure $P = (P_i + P_o)/2$. The effect of pressure on gain for two gas

mixtures is shown in fig. 4-4. Gas mixtures with lower He/CO₂ ratios were not considered due to arcing and discharge instability at higher pressure. Fig. 4-4 illustrates that the gain increases with increasing pressure until it reaches a maximum and then decreases due to increase in temperature [24]. At higher pressure, the discharge contracts to the cathode surface. At pressure greater than 8 torr (for the gas mixtures of 1:3.2:14.2 and 1:3.2:18), an increase in current is necessary to maintain the discharge covering the whole cathode.

Radial gain profile

The radial gain profiles across the waveguide (cathode) were measured for different gas mixtures at different discharge currents and pressures. The gains were nearly parabolic in shape. Fig. 4-5 through fig. 4-9 show the results of these measurements. These figures reveal that close to the cathode, at the end of the intense part of the negative glow, the gain increases with increasing distance from cathode until a maximum value is reached. Beyond this point, the gain decreases. The peaks of the gain curves increase and shift towards the cathode surface with increasing pressure and with a lower ratios of He/ CO₂ . The gain curves also are flattened somewhat with higher ratios of He/ CO₂ . This is important, since more uniform gain indicates better laser mode quality [36]. These measurements also revealed that an increase in the ratio of He/ CO₂ beyond 8 causes an increase in the intense part of the negative glow. Thus, shifting the gain onset away from the cathode surface and at the same time reducing the peak of the gain. Since the cathode has a circular hollow tube shape except a small segment of its cross-section was cut, the gain medium inside the cathode forms an almost cylindrical shape amplifier. The gain medium shape indicated better laser mode quality. The gain peaks are located between 2 and 4 mm from the bottom surface of the

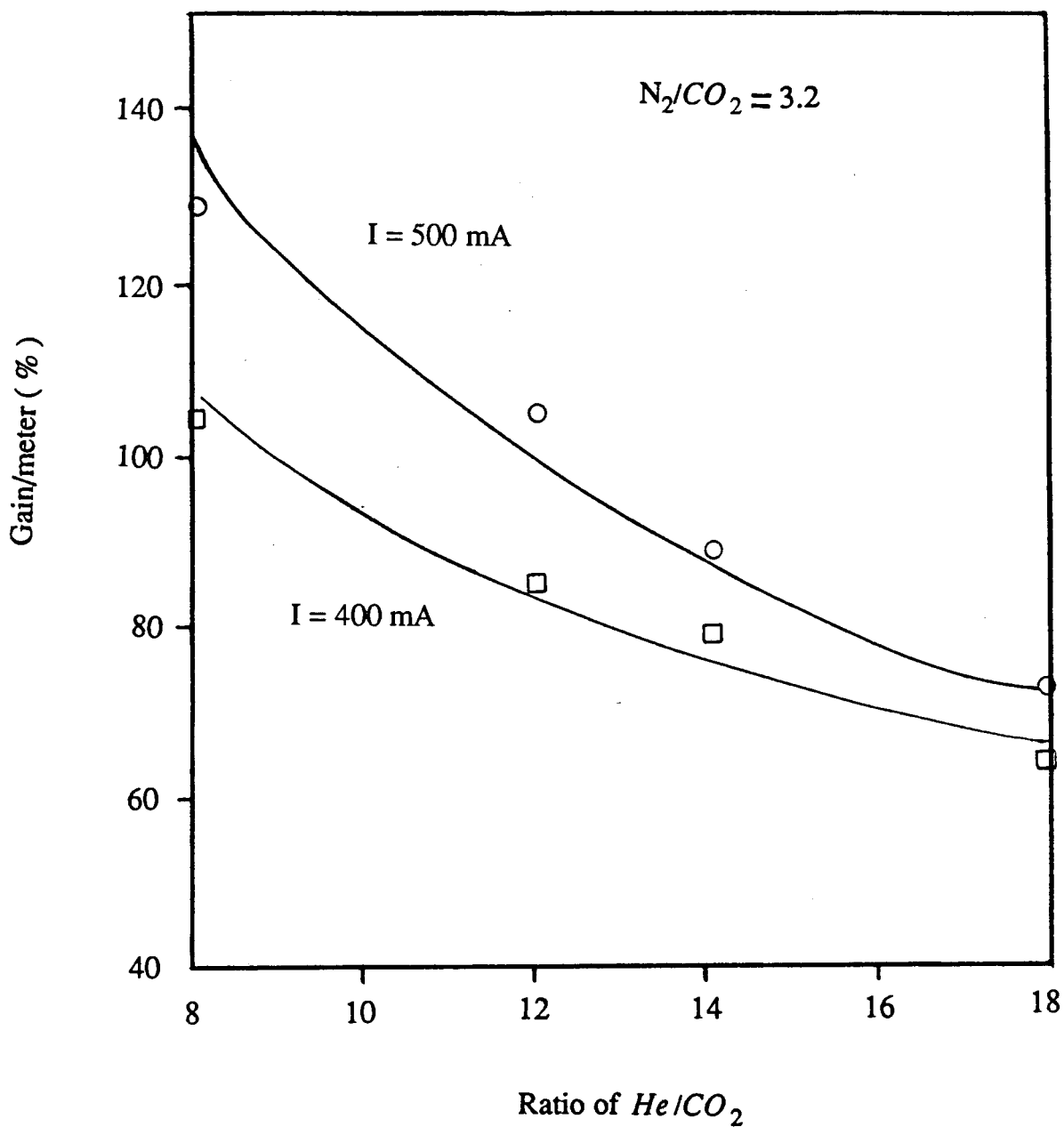


Figure 4-2. Gain as a function of He/CO₂ ratio at 7 Torr

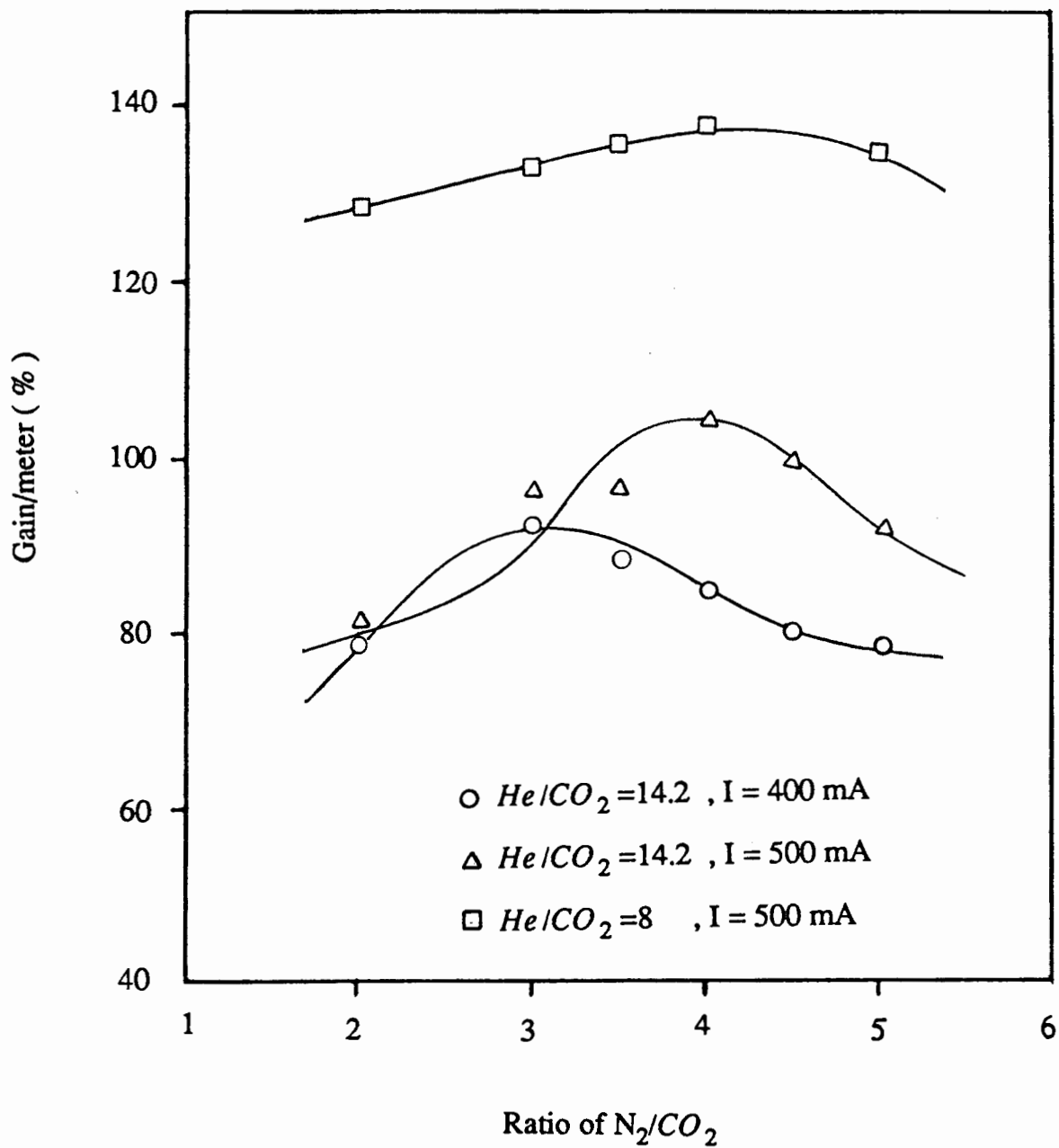


Figure 4-3. Gain as a function of N_2/CO_2 ratio at 7 torr

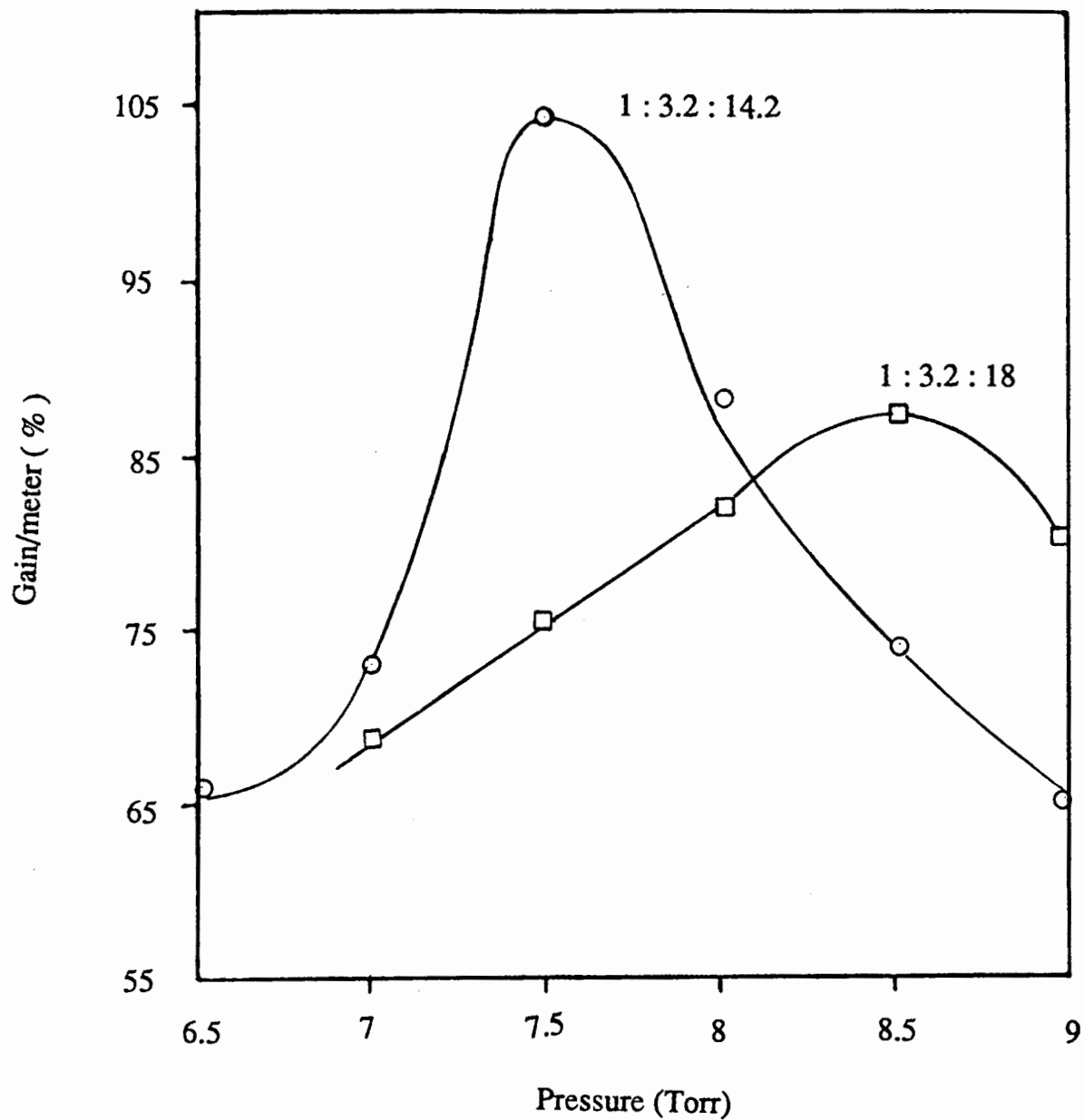


Figure 4-4. Gain as a function of pressure

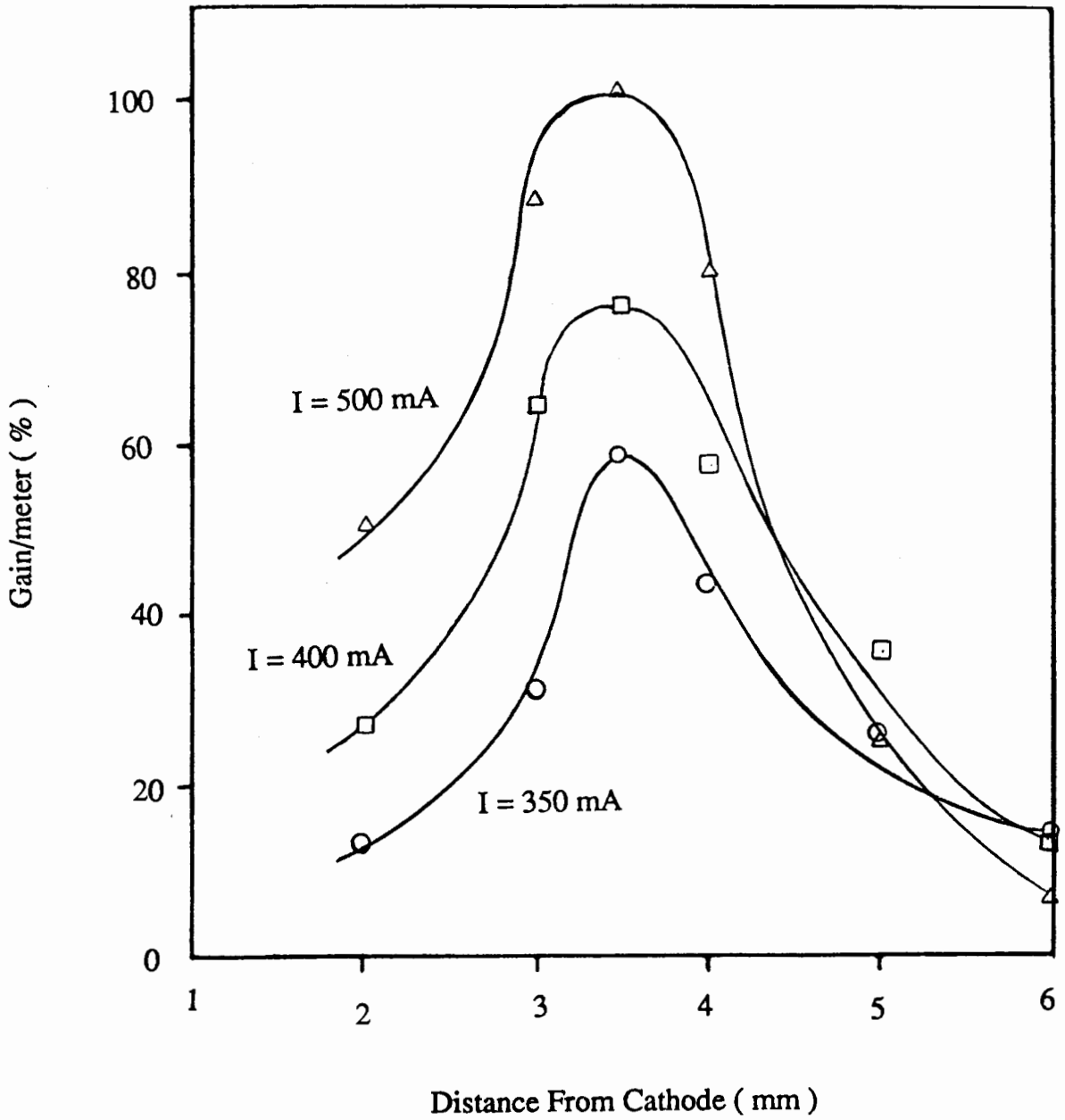


Figure 4-5. Gain profile for the gas mixture 1:3.2:14.2 at 7 torr

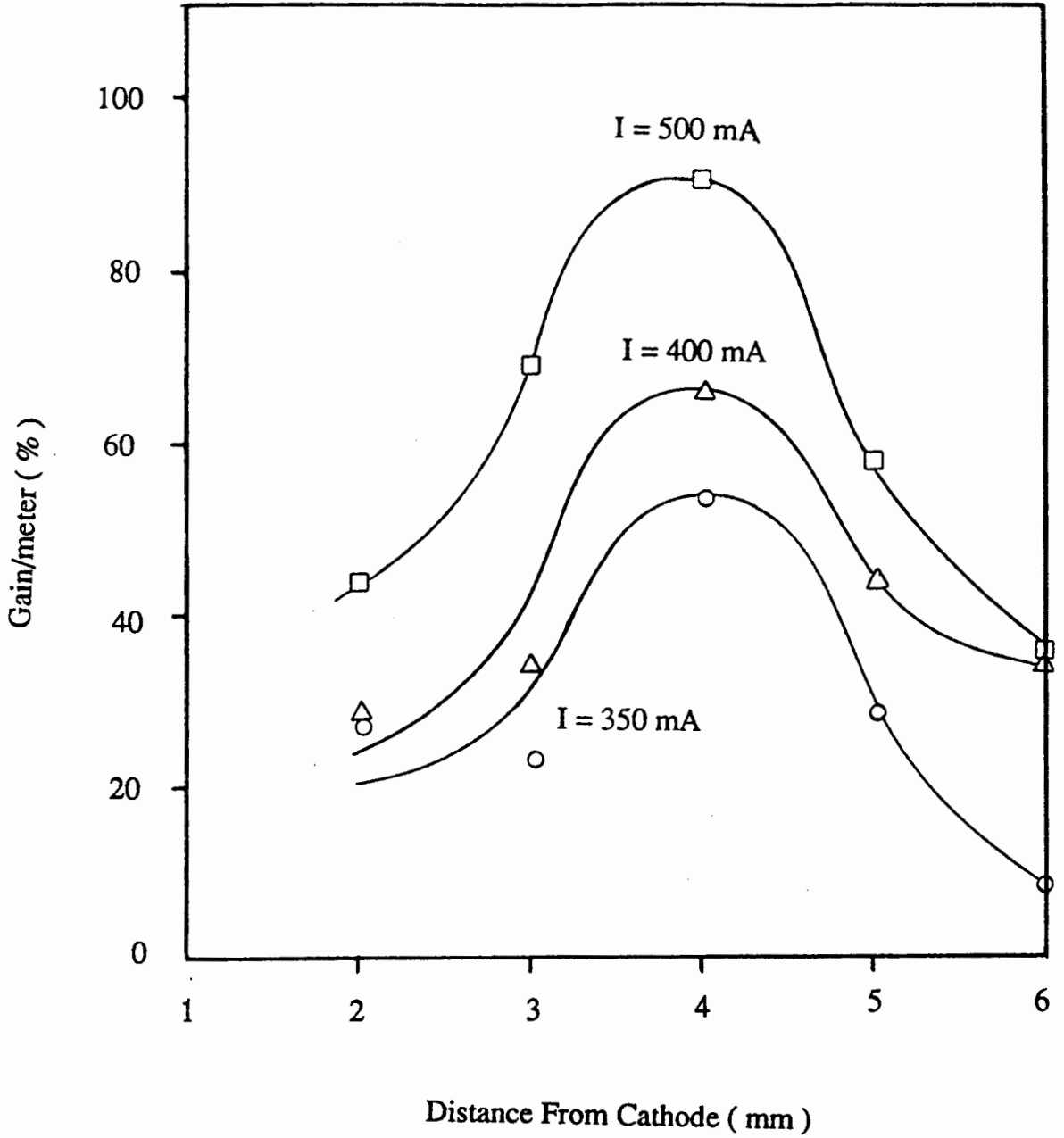


Figure 4-6. Gain profile for the gas mixture 1:3.2:14.2 at 6.5 torr

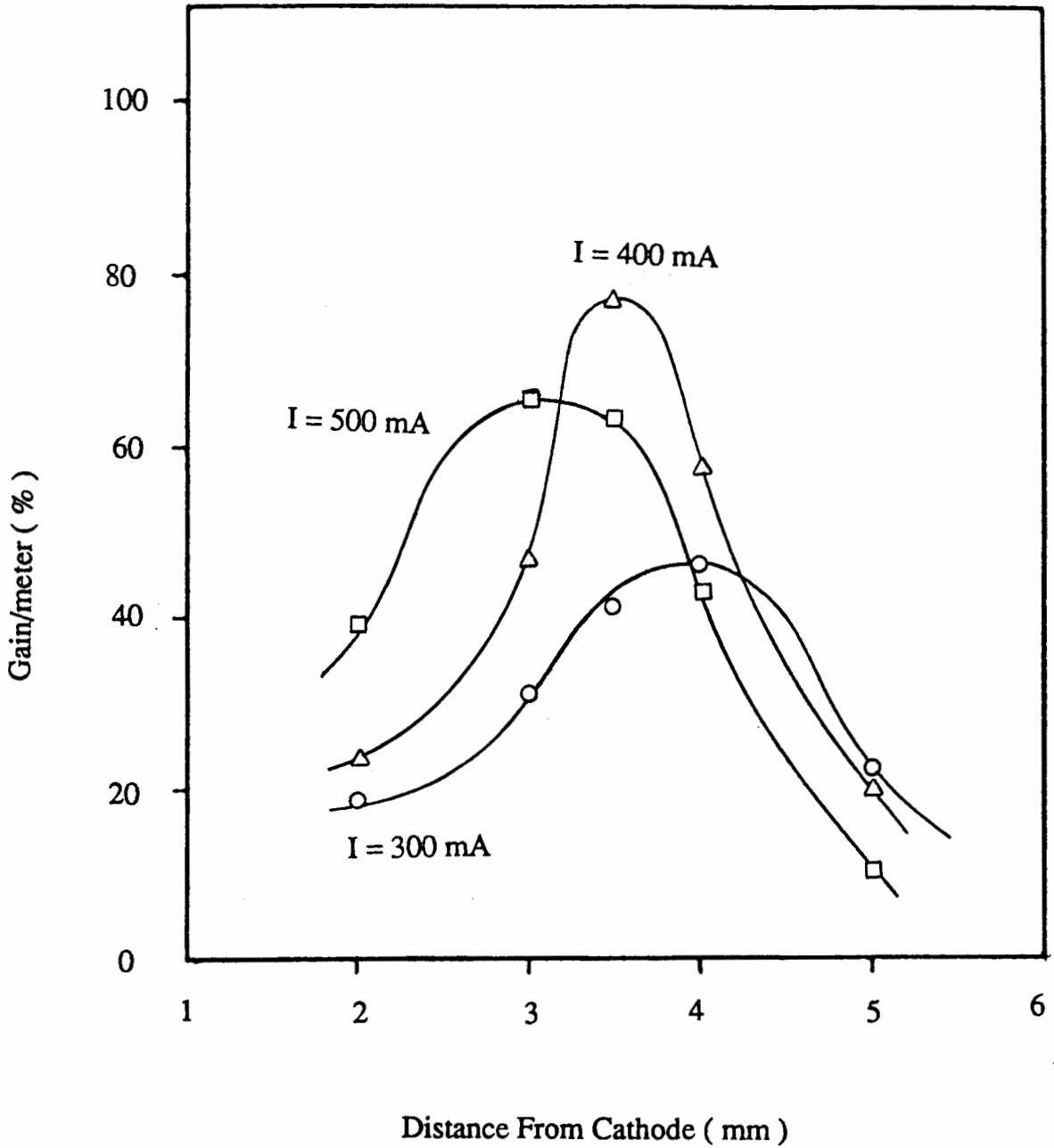


Figure 4-7. Gain profile for the gas mixture 1:3.2:18 at 7 torr

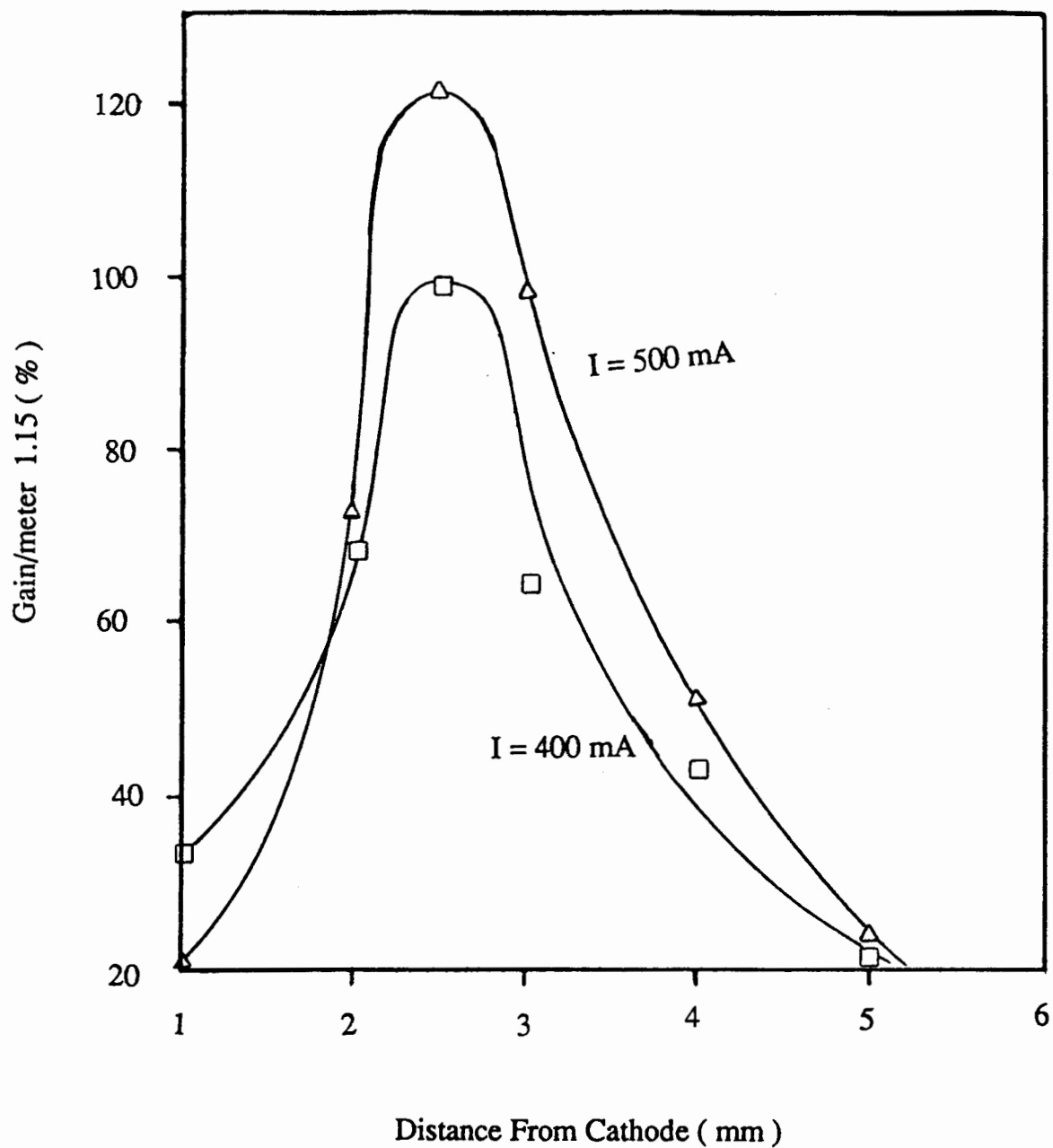


Figure 4-8. Gain profile for the gas mixture 1:3.2:8 at 7 torr

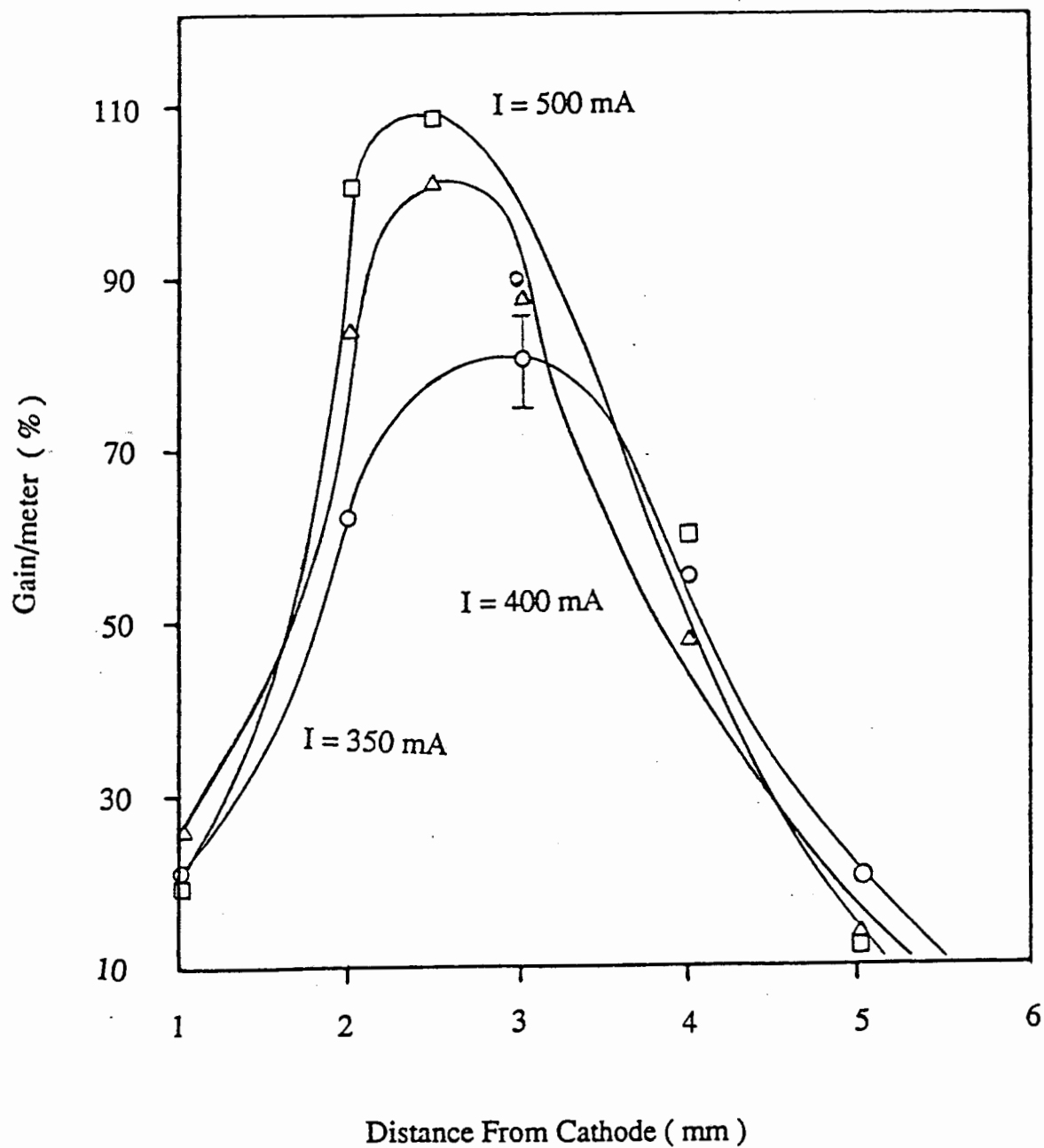


Figure 4-9. Gain profile for the gas mixture 1:3.2:8 at 6 torr

cathode.

Due to arcing, at higher currents, the range of currents were kept between 300 and 500 mA. The gain is found to increase with current in this range, except for the ratio 1:3.2:18 since the gain is lower at 500 mA than at 400 mA. This is maybe due to the increase in length of the intense part of the negative glow with current. Also, for a given E/N , this maybe due to the following reason. The average electron energy increases when the proportion of He is increased. This is because He has none of the inelastic vibrational losses that are present in CO_2 and N_2 . Thus, electron energies sufficient to excite the upper laser level occurs at lower E/N [38].

The previous measurements illustrate the availability of high gain and show that the optimum choice for gas mixture ratio and gas pressure are 1:3.2:14.2 of $\text{CO}_2 : \text{N}_2 : \text{He}$ and 7 torr respectively.

CHAPTER V

METAL WAVEGUIDE LASER

INTRODUCTION

The amplifier studied in the last chapter is turned into a laser medium by placing it inside an optical resonator. This optical resonator consists of two mirrors, one is a 1-m gold coated curved mirror and a flat germanium mirror with 95% reflectivity. The wave guide length is 42 cm and the distance between each mirror and the end of the waveguide is approximately 3-5 mm. The mirror spacing from the wave guide, which controls the coupling efficiency between the modes of the waveguide and the modes of free space, has been studied by Abrams et.al [39]. At this point, a problem that is worth mentioning is when we used an LH-41 coated mirror and a ZnSe mirror the coating burned in a few runs. The output modes and power will be the subject of this chapter.

WAVEGUIDE TRANSVERSE MODES

Theory

The modes of curved-concave metal waveguide have been described theoretically and experimentally by Casperson and Garfield [2] and by Marhic et.al [3,40]. They showed that these waveguide modes could be described in terms of Hermite-Gaussian functions parallel to the waveguide surface and Airy functions in the perpendicular direction. The results of their study will be presented. The coordinate system shown in fig. 5-1 will be used in this discussion. The major and

minor radii of curvature are $r_o \approx 46 \text{ m}$ and $R_o = 5.5 \text{ mm}$ respectively, r' is the distance perpendicular to the waveguide surface, z is the distance across the waveguide and ϕ is the angular distance along the waveguide.

Using this system of units the electric field is given by [2]

$$E_{mn}(r', \phi, z) = E_o F \left[\left[2 \frac{k_o^2}{r_o} \right]^{\frac{1}{3}} r' - \rho_n \right] H_m \left[\frac{\sqrt{2} z}{w_s} \right] \exp \left[\frac{z^2}{w_s^2} \right] e^{i(\psi - k_o z)} \quad (5.1)$$

where E_o is the normalizing factor, ρ_n is the n^{th} zero of the Airy function, k_o is the free space propagation constant, H_m is the Hermite-Gaussian function, ψ is a phase shift and w_s is the steady state spotsizes given by

$$w_s = \left[\frac{2(r_o R_o)^{1/2}}{k_o} \right]^{1/2} \quad (5.2)$$

If we neglect the effect of the waveguide walls on the propagating wave, then the output modes are Free space modes. The free space electric field is given by

$$E_{mn}(x, y, z) = E_o \frac{w_o}{w(z)} H_m \left[\frac{\sqrt{2} x}{w(y)} \right] H_n \left[\frac{\sqrt{2} z}{w(y)} \right] \exp \left[-ik_o \frac{x^2 + z^2}{2R(y)} - \frac{x^2 + z^2}{w^2(y)} \right] e^{i(k_o y + \psi)} \quad (5.3)$$

where $R(y)$ is the radius of curvature and $w(y)$ is the spotsizes of the beam at a distance y from the waist w_o and it is given by

$$w^2(y) = w_o \left[1 + \left[\frac{z}{z_o} \right]^2 \right] \quad (5.4)$$

$$w_o^2 = \frac{\lambda}{\pi} (dR)^{1/2} \left[1 - \frac{d}{R} \right] \quad (5.5)$$

$$z_o = \frac{\pi w_o^2}{\lambda} \quad (5.6)$$

where λ is the wave length, d is the cavity length and R is the radius of curvature of the curved mirror.

Fig. 5-2 and fig. 5-3 show the 2-D normalized intensity profile for the specified mode indices of Hermite-Gaussian and Airy functions respectively.

Experimental results and discussion

Since the laser beam is infrared, the cross-section of the beam is made visible by letting the beam strike a fluorescing surface of a thermal image plate. The output modes were always nearly perfect lower order modes because of the obstruction of the off-axis modes. This suggest that the gain in the middle of the waveguide, along the optical axis, is highest and decreases sharply away from it. Also, the cathode-anode separation acts as an aperture.

At low current and pressure of 600 mA and 7 torr respectively, the output modes were free-space lower order Hermite-Gaussian modes. At higher current and pressure, 900 mA and 10 torr respectively, the modes were low order Airy-Hermite-Gaussian modes. This difference in modes shape could be explained as follows: at low current and pressure, the thickness of the gain medium is smaller than the distance between the gain medium and the waveguide surface . This makes it almost impossible to make the beam use the waveguide surface as a guiding medium because the medium between the gain medium and the waveguide walls is thick and lossy. But at high current and pressure, the gain is high and its thickness is large compared to its separation from the waveguide surface. Therefore, the system lases even when the mirrors are tilted, with a small angle to make the beam reflect from the waveguide surface. As a result, we get the waveguide modes.

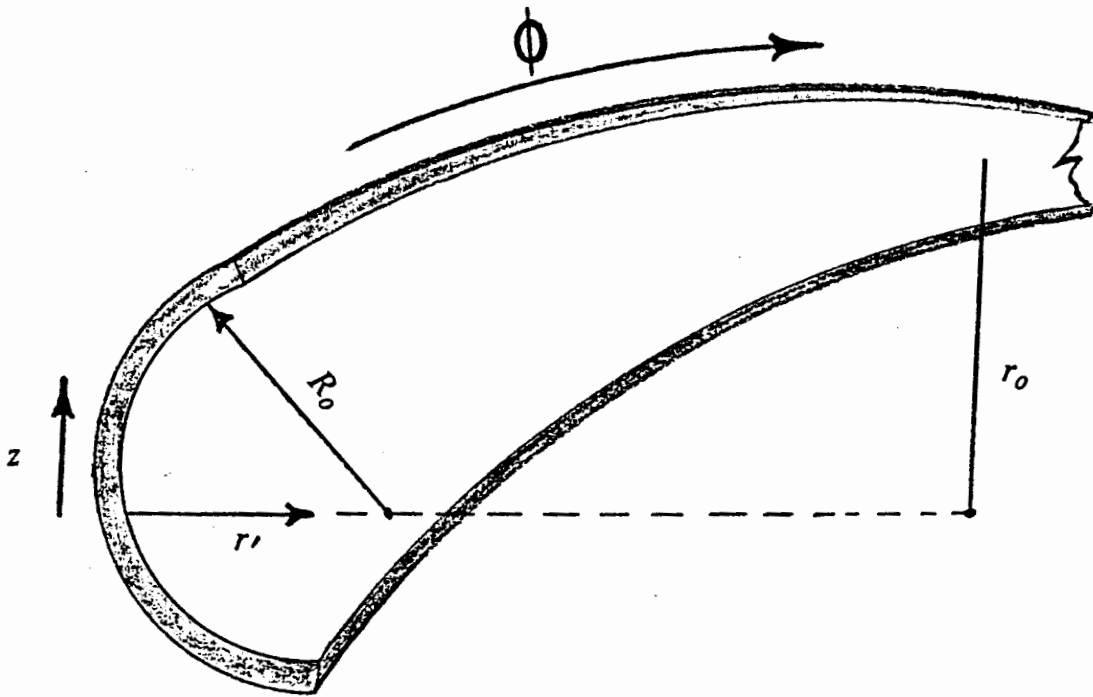


Figure 5-1. Waveguide coordinate system

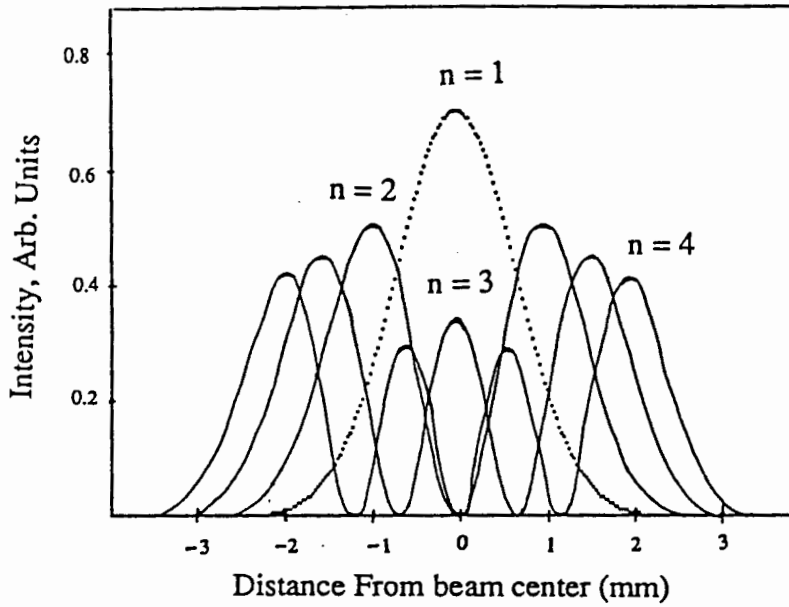


Figure 5-2. Normalized intensity profile for the second order Hermite-Gaussian mode

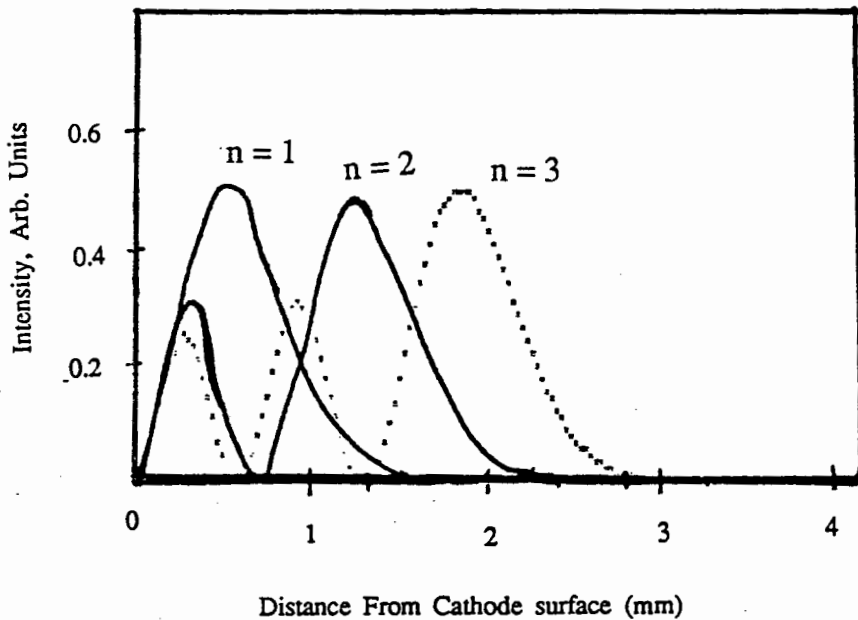


Figure 5-3. Normalized intensity profile for the second order Airy mode

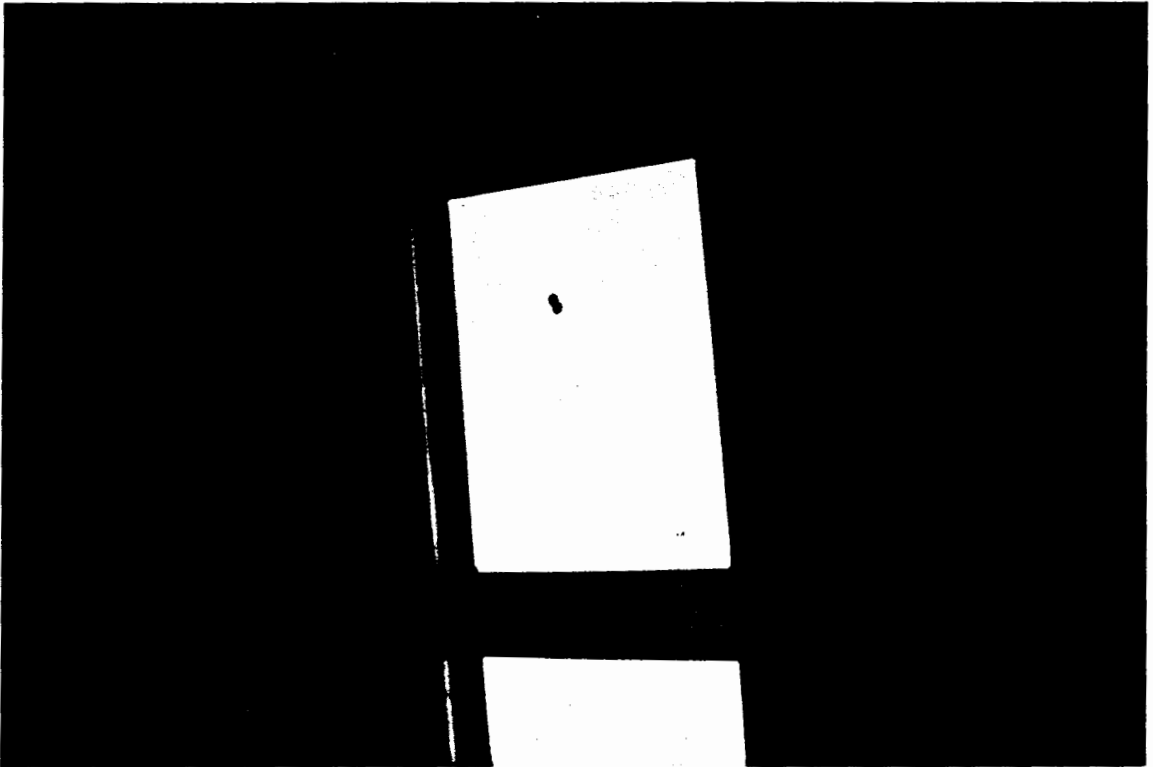


Figure 5-4. First order Hermite-Gaussian transverse output modes when incident on thermal image plate .2m from output coupler

Figure 5-4 shows a pictures of the first order Hermite-Gaussian output laser modes at low pressure and current. At high pressure and current, it was not possible to take pictures due to the arcing, which damages the waveguide, at these operation conditions.

OUTPUT POWER

One of the most important measurements needed to determine the operation characteristics is the power dependence on current. Therefore, the laser's output power was measured as a function of current for different gas mixtures and pressures. These measurements were done using a SCIENTECH model 362 power meter.

Figure 5-5 shows that at 7 torr, the power is almost linearly proportional to the current up to 600 mA for the different gas mixtures shown. But for higher current or current and pressure, figure 5-6 illustrates that the power increases less with current. The reasons for this behavior may be due to increase in temperature and fast rate of gas contamination. Finally, for the same gas mixture ratio, flow rate and energy input, the efficiency of the wave guide laser is the same or better than that for longitudinal laser used in our gain measurement.

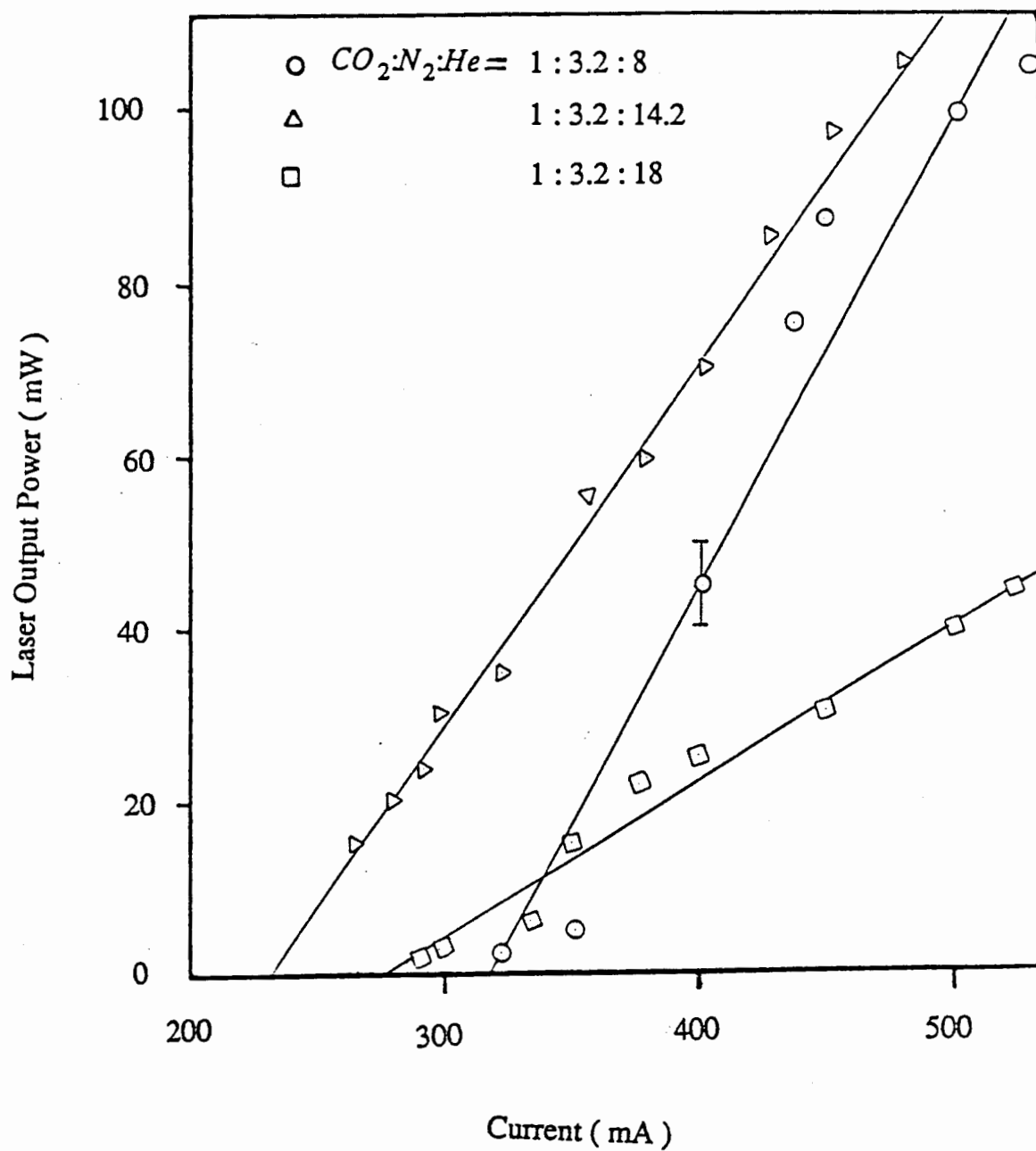


Figure 5-5. Laser power as a function of current for different gas mixtures at 7 torr

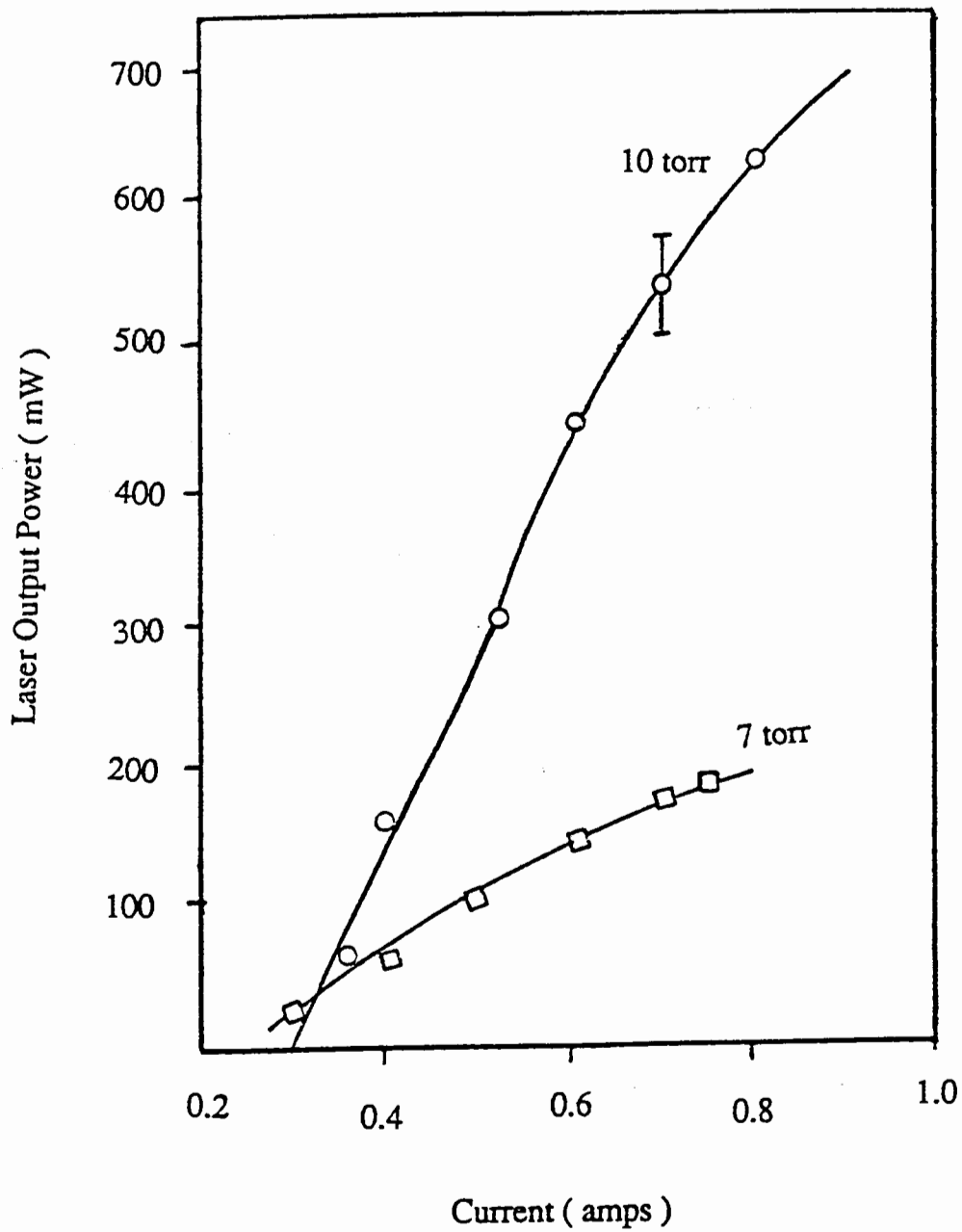


Figure 5-6. Laser power as a function of current for the gas mixture 1:3.2:14.2 at 7 torr and 10 torr

CHAPTER VI

CONCLUSION AND RECOMMENDATIONS

CONCLUSION

The design and operation of a DC-excited cw CO₂ metal waveguide laser, in which a slotted hollow-cathode in a transverse discharge also doubles as a metal waveguide has been presented. The experimental results have indicated, for the first time, the high optical gain available using the new cathode design as a CO₂ laser amplifier. The resulting transverse discharge has many advantages which include low voltage excitation, positive impedance, discharge homogeneity along the optical axis and the unexpected high gain of the special FDS formed along the center of the cathode. Another attractive feature is the high thermal conductivity of the cathode walls which increases the optical gain. The discharge was found to be stable at ratios of He/ CO₂ higher than 8. As a result of this investigation, the gain was found to increase with current and pressure.

Lasing has been achieved using the above amplifier. The output transverse modes are found to be clean and smooth lower order modes due to the uniformity and shape of the gain medium which obstruct the formation of off axis modes. These modes were found to be free space modes when the mirrors are parallel to each other. Since the waveguide is also bent along the optical axis, it is possible to obtain a waveguide modes that agree with the theoretical Airy-Hermite-Gaussian functions under two conditions. The gain medium must fill almost the

whole waveguide and the mirrors must be perpendicular to the waveguide axis. A maximum TEM_{00} power output of 1 watt was obtained.

RECOMMENDATIONS FOR FUTURE WORK

At this stage, it is very reasonable to expect that our device is capable of delivering higher power with higher efficiency after a few adjustments. Therefore, for further research and development of this DC-excited metal waveguide lasers, it is necessary to identify the parts of the device that need to be developed or redesigned to meet a particular application. Since this device is in its infant stage and is being built for laboratory studies, it needs further engineering before it can be used in practical applications.

The following are some suggestions to improve the power and efficiency of this laser:

1. Reducing the size of the laser structure, so that most of the flowing gas will be contained in the waveguide amplifying medium.
2. To minimize arcing, reduce the field gradient at the edges of the electrodes especially the cathode by machining smoother and cleaner edges. Another suggestion, which needs careful investigations before implementation, is to use a hollow-cathode with the anode inside the cathode.
3. Increase the flow rate.
4. To make the laser operate sealed off, the addition of a low ionizing potential gas such as xenon is required.

REFERENCES

- [1] E. Garmire, T. McMahon and M. Bass, "**Propagation of Infrared Light in Flexible Hollow Waveguides,**" *Appl. Opt.*, vol. 15, pp. 145-150, Jan. 1976.
- [2] L. W. Casperson and T. S. Garfield, "**Guided Beams in Concave Metallic Waveguides,**" *IEEE J. Quantum Electron.*, vol. QE-15, pp. 491-496, June 1979.
- [3] M. E. Marhic, L. I. Kwan and M. Epstein, "**Whispering-Gallery CO₂ Laser,**" *IEEE J. Quantum Electron.*, vol. QE-15, pp. 487-490, June 1979.
- [4] D. A. Pinnow et.al., "**Polycrystalline Fiber Optical Waveguides for Infrared Transmission,**" *Appl. Phys. Lett.* vol. 33, pp. 28-29, July 1978.
- [5] Y. Mimura and C. Ota, "**Transmission of CO₂ Laser Power by Single-Crystal CsBr Fibers,**" *Appl. Phys. Lett.* vol. 40, pp. 773-775, May 1982.
- [6] J. G. Grossman, L. W. Casperson and O. M. Stafsudd, "**Radio-Frequency-Excited Carbon Dioxide Metal Waveguide Laser,**" *Appl. Opt.*, vol. 22, pp. 1298-1305, May 1983.
- [7] P. K. Cheo, "**CO₂ Lasers,**" *Lasers: A Series of Advances*, A. Levine and A. Demaria, M. Dekker, New York, 1971, p. 111-262. .sp
- [8] G. Bekefi, *Principles of Laser Plasmas*, J. Wiley, New York, 1979.
- [9] A. J. Demaria, "**Review of cw High-Power CO₂ Lasers,**" *Proc. of IEEE*, vol. QE-61, pp. 731-748, June 1973.
- [10] W. W. Duley, "**The CO₂ Laser,**" *CO₂ Lasers : Effects and Applications*, Academic Press, New York, 1976, p. 58.
- [11] J. T. Verdeyen, "**Laser Excitation,**" *Laser Electronics*, Pentic-Hall, New Jersey, 1981, p. 252-303.
- [12] M. J. W. Boness and G. J. Schulz, "**Vibrational Excitation of CO₂ by Electron Impact,**" *Phys. Rev. Lett.*, vol. 21, pp. 1031-1034, Oct. 1968.
- [13] G. J. Schulz, "**Vibrational Excitation of N₂ , CO and He by Electron Impact,**" *Phys. Rev.*, vol. 135A, pp. 988-994, 1964.

- [14] M. J. Boness and G. J. Schulz, "**Vibrational Excitation in CO₂ via The 3.8-eV Resonance,**" Phys. Rev., vol A9, pp. 1969-1975, May 1974.
- [15] W. L. Nighan, "**Electron Energy Distributions and Collision Rates in Electrically Excited N₂, CO and CO₂ ,**" Phys. Rev. (A), vol. 2, pp.1989-1999, Nov. 1970.
- [16] W. L. Nighan and J. H. Bennett, "**Electron Energy Distribution Functions and Vibration Rates in CO₂ Laser Mixtures,**" Appl. Phys. Lett., vol. 14, pp. 240-243, Apr. 1969.
- [17] G. Francis, *Handbuck der Physik*, vol. XXII, Springer, Berlin, 1956.
- [18] A. V. Engel, *Ionized Gases*, Oxford Univ. Press, London, 1955.
- [19] N. Essam, *Fundamental of Gaseous Ionization and Plasma Electronics*
- [20] C. K. N. Patel, "**Contineous-Wave Laser Action on Vibrational-Rotational Transitions of CO₂ ,**" Phys. Rev., vol. 136, pp. A1187-A1193, 1964.
- [21] R. J. Frieberg and P. O. Clark, "**CO₂ Transverse Discharge Lasers,**" IEEE J. Quantum Electron.(Corresp.), vol. QE-7, pp. 581-583, Dec. 1971.
- [22] G. Sedgwick and H. Seguin, "**Low Voltage CO₂ Laser Excitation,**" Appl. OPT., vol. 9, Dec. 1970.
- [23] M. A. Aboobaker, **Properties of Coaxial Discharge Carbon Dioxide Laser Amplifier**, M.S. in Engineering, Electrical Sciences and Engineering Dept., University of California, Los Angeles, 1973.
- [24] K. T.-K. Cheng and L. W. Casperson, "**Properties of a Coaxial cw CO₂ Laser,**" Appl. Opt., vol. 18, pp. 2130-2135, July 1979.
- [25] C. S. Willet and G. M. Janny, "**Amplification at 10.6 μ in the Negative Glow of Hollow Cathode Discharge in a CO₂ - He Mixture,**" IEEE J. Quantum Electron., vol. QE-6, pp. 568-569, Sept. 1970.
- [26] D. J. Sturges and H. J. Oskam, "**Hollow-Cathode Discharge in Hydrogen and Noble Gases,**" J. Appl. Phys., vol. 37, pp. 2405-2412, May 1986.
- [27] R. F. Little and A. V. Engel, "**The Hollow-Cathode Effect and Theory of Glow Discharge,**" Proc. Roy. Soc., vol. A224, pp. 209-227, 1954.
- [28] K. Fujii et.al., "**Design of Whitelight Laser Based on Cathode Fall Theory,**" IEEE J. Quantum Electron., vol. QE-15, pp. 35-43, Jan. 1979.

- [29] S. Hashiguchi and M. Hasikuni, "Theory of the Hollow Cathode Glow Discharge," *Jpn. J. Appl. Phys.*, vol. 26, pp. 271-280, Feb. 1987.
- [30] V. P. Chebotayev, "Operating Condition of an Optical Maser Containing a He-Ne Mixture," *Radio Engrg. Electron. Phys. (USA)*, vol. 10, pp. 314-316, 1965.
- [31] S. C. Wang and A. E. Siegman, "Hollow-Cathode Transverse Discharge He - Cd⁺ Lasers," *Appl. Phys.*, vol. 2, pp. 143-150, 1973.
- [32] L. M. Kureja, R. k. Khare and U. K. Chatterjee, "Longitudinal CO₂ Laser Operating at Line Voltage with Hollow-Cathode Discharge," *Rev. Sci. Instrum.*, vol. 57, pp. 1689-1691, Aug. 1986.
- [33] G. J. M. Ahsmann, "Some remarks on the Anodefall in the FDS," L. B. Loeb, *Fundamental Process of Electrical Discharge in Gases*, John Willey and Sons, 1947, p. 306.
- [34] L. W. Casperson, Lecture notes.
- [35] E. T. Gerry and D. A. Leonard, "Measurement of 10.6 microns CO₂ Laser Transition Probability and Optical Broadening Cross Section," *Appl. Phys. lett*, vol. 8, pp. 227-229, May 1966.
- [36] V. A. Seguin, et.al., "Gain Characteristics of a MAGPIE Coaxial CO₂ Laser System," *IEEE J. Quantum Electron.*, vol. QE-23, pp. 600-604, May 1987.
- [37] A. E. Siegman, *An Introduction to Laser and Maser*, McGraw-Hill, New York, 1968, ch. 3.
- [38] J. J. Lowke, A. V. Pheleps and B. W. Irwin, "Predicted Electron Transport Coefficients and Operating Characteristics of CO₂-N₂-He Laser Mixture," *J. Appl. Phys.*, vol. 44, pp. 4664-4471, 1973.
- [39] R. L. Abrams and A. N. Chester, "Resonator Theory for Hollow Waveguide Lasers," *Appl. Opt.*, vol. 13, pp. 2117-2125, Sept. 1974.
- [40] M. E. Marhic, L. I. Kwan and M. Epstein, "Optical Surface Waves Along a Toroidal Metallic Guide," *Appl. Phys. lett*, vol. 33, pp. 609-611, Oct. 1979.